

# Summary of the High Ice Water Content (HIWC) RADAR Flight Campaigns

Thomas P. Ratvasky<sup>1</sup>, Steven D. Harrah<sup>2</sup>, J. Walter Strapp<sup>3</sup>, Lyle E. Lilie<sup>4</sup>, Fred H. Proctor<sup>2</sup>, Justin K. Strickland<sup>5</sup>, Patricia J. Hunt<sup>5</sup>, Kristopher Bedka<sup>2</sup>, Glenn Diskin<sup>2</sup>, John B. Nowak<sup>2</sup>, T. Paul Bui<sup>6</sup>, Aaron Bansemer<sup>7</sup>, Chris Dumont<sup>8</sup>

<sup>1</sup> NASA Glenn Research Center, <sup>2</sup> NASA Langley Research Center, <sup>3</sup> Met Analytics Inc., <sup>4</sup> Science Engineering Associates, <sup>5</sup> Analytical Mechanics Assoc., <sup>6</sup> NASA Ames Research Center, <sup>7</sup> National Center for Atmospheric Research, <sup>8</sup> FAA William J. Hughes Technical Center

## Abstract

NASA and the FAA conducted two flight campaigns to quantify onboard weather radar measurements with in-situ measurements of high concentrations of ice crystals found in deep convective storms. The ultimate goal of this research was to improve the understanding of high ice water content (HIWC) and develop onboard weather radar processing techniques to detect regions of HIWC ahead of an aircraft to enable tactical avoidance of the potentially hazardous conditions. Both HIWC RADAR campaigns utilized the NASA DC-8 Airborne Science Laboratory equipped with a Honeywell RDR-4000 weather radar and in-situ microphysical instruments to characterize the ice crystal clouds. The purpose of this paper is to summarize how these campaigns were conducted and highlight key results.

The first campaign was conducted in August 2015 with a base of operations in Ft. Lauderdale, Florida. Ten research flights were made into deep convective systems that included Mesoscale Convective Systems (MCS) near the Gulf of Mexico and Atlantic Ocean, and Tropical Storms Danny and Erika near the Caribbean Sea. The radar and in-situ measurements from these ten flights were analyzed and correlations defined. Key results included 1) derived relationships between radar reflectivity factor (RRF), Ice Water Content (IWC), and ice particle size distributions, 2) characterization of HIWC conditions at the -50°C and other flight levels, and 3) verification of pilot observations, such as low radar reflectivity factor and pitot and total air temperature (TAT) anomalies. This data set also enabled new pilot radar HIWC detection algorithms to be developed and tested.

A second campaign was conducted in August 2018 to test proposed HIWC radar detection algorithms within a new set of storm systems. Seven research flights were conducted from bases of operations in Ft. Lauderdale, Florida; Palmdale, California; and Kona, Hawaii. Flights were made into convective systems over the Gulf of Mexico and into an eastern-Pacific tropical system that developed into Hurricane Lane. Using a new, NASA-developed radar processing technique called “Swerling”, regions of HIWC were identified, and estimates of IWC were produced, at distances up to 60 Nm ahead of the NASA DC-8. Subsequently, the DC-8 flew through these regions to acquire the in-situ measurements to verify the radar-based IWC estimates.

## Introduction

In 2003, the FAA chartered an Aviation Rulemaking Advisory Committee (ARAC) called the Engine Harmonization Working Group (EHWG) to evaluate the effects of supercooled large drop (SLD) and

mixed phase/glaciated conditions on commercial transport power plants [1]. The EHWG found that most weather-related engine power-loss events on commercial aircraft had occurred in or near deep convective storms. Mason, et al. [2] evaluated 46 such power-loss or engine core damage events, and concluded that these events were caused by ingestion of high mass concentrations of ice crystals into the engine core flow path. It was argued that the ingested ice crystals could change phase, refreeze, and block airflow through the engine or shed into the compressor causing damage. Mason, et al. also found that the power-loss events were usually occurring in regions with no significant flight radar echoes (only black or green on pilots radar display) at flight altitude. The lack of radar reflectivity factor at flight level was attributed to clouds consisting of small ice crystals, which are inefficient radar scatterers.

The EHWG developed a Mixed-Phase/Glaciated Icing Technology Plan [3] that formed the basis for much of the ice crystal icing research and development that followed. Task 2 of this plan was to *conduct flight test research to characterize the high ice water content environments*. In 2006, this task initiated the High Ice Water Content (HIWC) Study, which was an international collaboration of NASA, FAA, Environment Canada, National Research Council Canada, Australian Bureau of Meteorology, National Center for Atmospheric Research, and the Boeing Company. The HIWC Science Plan [4] was written to define the aviation and atmospheric science objectives of a flight test campaign to collect cloud in-situ data for Task 2. One objective was to investigate the use of onboard weather radar to detect HIWC conditions so that pilots could make tactical decisions to avoid the HIWC environment.

In 2012, the European High Altitude Ice Crystal (HAIC) project and HIWC project initiated collaborations to conduct the flight research defined in the HIWC Science Plan and in the HAIC-SP2 Description of Work [5]. Two HAIC-HIWC flight campaigns were conducted using the SAFIRE Falcon-20 equipped with in-situ icing cloud microphysical and icing instruments, the RASTA 95-GHz research radar, and a Honeywell Primus 660 pilot weather radar. The first HAIC-HIWC campaign was conducted from Darwin Australia in January-March 2014. The second HAIC-HIWC campaign was conducted from Cayenne, French Guiana in May 2015. Forty flights were accomplished which led to a substantial and unique compilation of cloud in-situ microphysics data, and remote sensing data from the RASTA radar, in HIWC conditions [6, 7, 8]. However, the Primus 660 radar on the Falcon-20 only supported noncoherent signal processing and had no means to record the fundamental radar measurements. As a result, only display radar imagery was acquired. Leroy et al. [7] commented that the Falcon-20 pilot radar indicated relatively low reflectivity (“no echoes or green echoes, i.e. radar reflectivity factor

less than 32 dBZ”) at flight level during the 2014 HAIC-HIWC flight campaign. Analysis of the Primus 660 radar display bus recordings and IWC measured by an Iso-Kinetic Probe (IKP2) was performed to derive histograms of the reflectivities for three bands of TWC. Approximately 94% of RRFs observed in HIWC conditions during the 2014 HAIC-HIWC flight campaign were displayed as black ( $\text{dBZ} < 22$ ) and green ( $22 < \text{dBZ} < 32$ ) (Figure 1). These results were consistent with commercial pilot reports [2] and confirmed the observations in Leroy et al. [7].

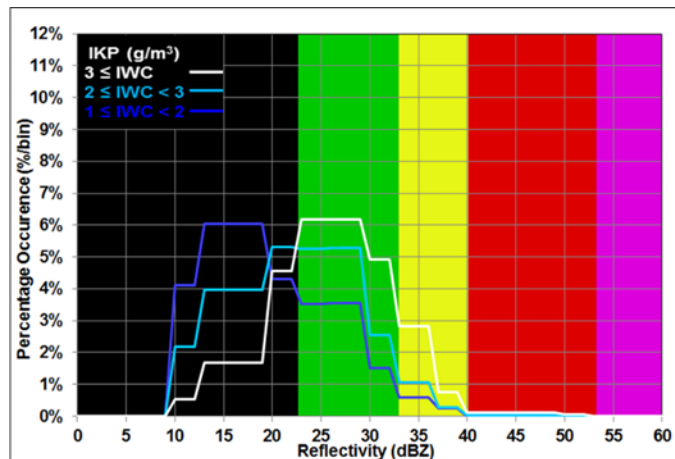


Figure 1. Percentage of occurrence per bin of radar reflectivity from 2014 HAIC-HIWC Darwin Campaign. Radar display data courtesy of SAFIRE

After the Darwin 2014 HAIC-HIWC flight campaign, NASA and the FAA initiated plans to conduct the HIWC RADAR flight campaign with the primary objective to quantify onboard weather radar measurements with in-situ measurements of high concentrations of ice crystals found in deep convective storms. The effort resulted in two HIWC RADAR flight campaigns. The purpose of this paper is to summarize how these campaigns were conducted and highlight key results.

## HIWC RADAR I (2015)

The primary goal of this flight campaign was to collect unprocessed radar return signals (i.e. “In-phase and Quadrature” (I&Q) sample data) and cloud microphysics data in HIWC conditions in order to subsequently develop correlations between the radar data and the levels of IWC. A secondary goal was to collect additional cloud microphysical data at the  $-50^{\circ}\text{C}$  flight level in order to augment the characterization data collected through the HAIC-HIWC flight campaigns.

### NASA DC-8 with HIWC Instrumentation

The NASA DC-8 (NASA 817) is an airborne research laboratory used for earth, atmospheric, and space science missions. The DC-8 is a four-engine, jet aircraft with a range of 5,400 Nm (10,000 km), a ceiling of 41,000 ft. (12,500 m), and a maximum flight duration of 12 hours. The aircraft has been highly modified to accommodate a wide variety of flight research experiments. These modifications include special power systems, viewports, wing pylons, window blanks and fuselage panels to mount instruments and probe heads to measure in-situ and remote conditions. These capabilities met or exceeded the HIWC RADAR flight requirements.

Prior to the 2015 flight campaign, the DC-8 was configured with the Honeywell RDR-4000 radar and cloud microphysical in-situ

instrumentation. Identification and location of these sensors are shown in Figure 2.

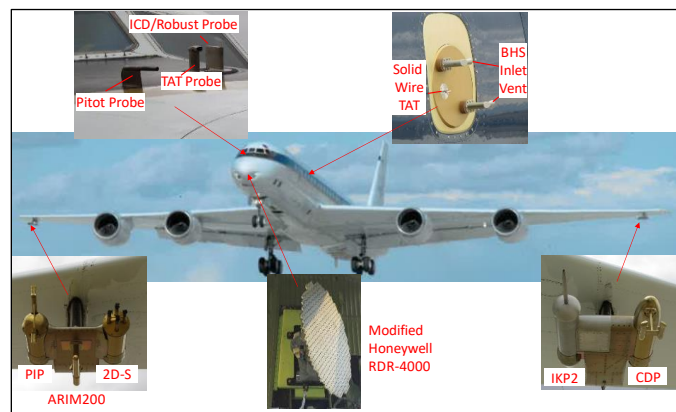


Figure 2. General layout of DC-8 with HIWC RADAR instrumentation

The Honeywell RDR-4000 was a commercial-off-the-shelf, X-band weather radar, with a 24” antenna, pedestal, and radar processor that interfaced to a DC-8 multi-function display unit. A Honeywell CertPort Recorder was interfaced to the radar processor to record the unprocessed radar I&Q data. NASA data systems processed the I&Q data and provided customized displays of the radar data to the NASA radar researchers and DC-8 crewmembers (Figure 3). Radar data was displayed at four horizontal levels: 2,500 ft. above flight level, at flight level, and 5,000 ft. and 10,000 ft. below flight level.

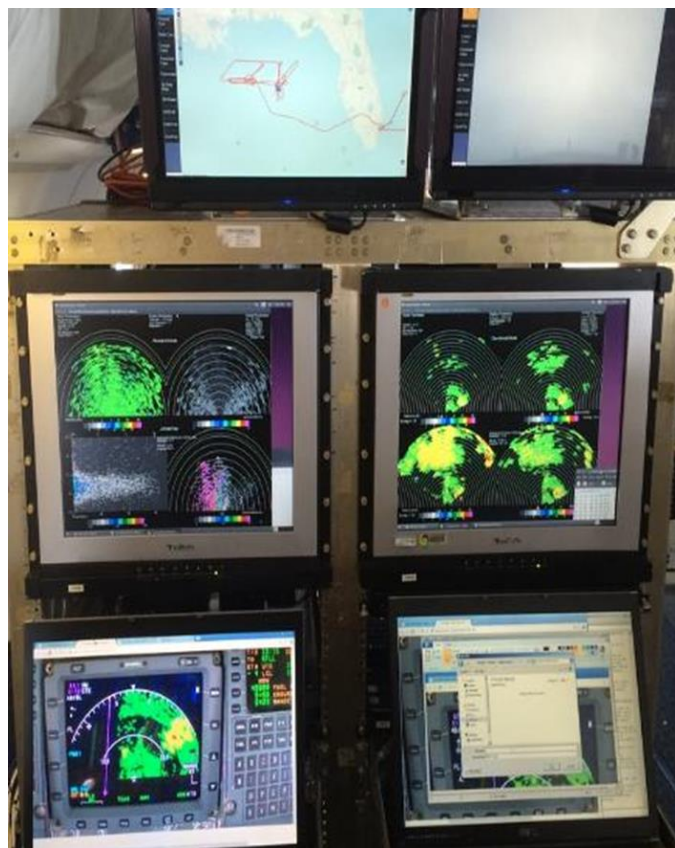


Figure 3. HIWC RADAR displays

The primary ice cloud parameters of interest for the radar correlations were the bulk IWC and the ice cloud particle size distribution (PSD).



To that end, the icing instruments used on the DC-8 were the same as those used on the SAFIRE Falcon 20 during the HAIC-HIWC flight campaigns. Bulk IWC was measured with the Iso-kinetic Probe 2 (IKP2), a Total Water Content (TWC)<sup>1</sup> evaporator probe [9, 10]. The IKP2 was mounted on the left wing pylon at the inboard position. To support the IKP2 TWC calculations, a Background Humidity System (BHS) using a Licor LI840A was mounted in the cabin, but sampled the ambient air through an inlet on a window blank near station 530. Particle size distributions were measured using the following three instruments:

- DMT Cloud Droplet Probe (CDP-2) [2-50  $\mu\text{m}$ ]
- SPEC 2D-S imaging probe [10-1280  $\mu\text{m}$ ]
- DMT Precipitation Imaging Probe (PIP) [100-6200  $\mu\text{m}$ ]

The CDP-2 was mounted on the left wing pylon, outboard position on a canister nosecone. The 2D-S was mounted on the right wing pylon, inboard position and the PIP was mounted on the right wing pylon, outboard position. All particle probes used anti-shattering tips to reduce measurements of shattered ice artifacts [11, 12].

Additional measurements were made to support the primary and ancillary analyses. For example, airspeed, air temperature (total and static), pressure altitude, GPS location etc. were all provided by DC-8 standard systems. A research total air temperature (TAT) probe and a Science Engineering Associates (SEA) TWC hot-wire probe were also mounted on the fuselage nose in order to investigate localized ice concentration factors and potential for TAT and pitot probe anomalies. Likewise, a solid-wire TAT probe with no de-ice heating was mounted to the same window blank as the BHS to provide a baseline TAT that would not be subject to TAT anomalies. An L3 Stormscope WX-1000E was also integrated on the DC-8 to provide lightning detection information to the flight crew and research team.

## 2015 Campaign Planning and Operations

After the decision was made to use the NASA DC-8 for the 2015 flight campaign, coordination meetings with NASA Armstrong, Langley, Glenn, and the FAA were held to discuss instrumentation requirements, base of operations, flight sampling strategies, concepts of operations, and mission rules and flight procedures. The following sections provide the details on these topics.

### Base of Operations and Operating Area:

Potential basing options were considered with respect to the NASA DC-8 availability and funding levels. Climatology studies of the Caribbean, Gulf of Mexico, and eastern Pacific were conducted. With these constraints, it was determined that a 3-week, 80 flight-hour campaign could be conducted in August 2015 within the USA and its territories. The original plan was to conduct the campaign from Aguadilla, Puerto Rico. However, due to persisting drought conditions in the Caribbean during July 2015, the base of operations was reset to Ft. Lauderdale, Florida (KFL) just weeks prior to the start of the deployment.

The Operating Area (Figure 4) was defined to coordinate with Air Traffic Control (ATC) Flight Information Regions (FIR) and to establish diplomatic clearances to transit airspace controlled by non-

US governments. The range and endurance of the DC-8 enabled the boundaries of the operating area to be quite extensive. Research operations were limited to convective systems that developed over water.

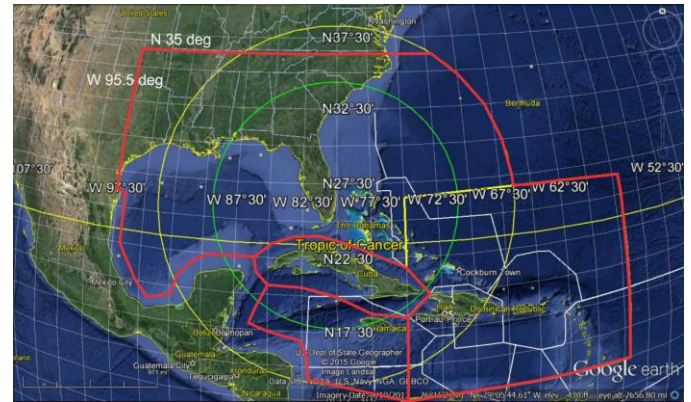


Figure 4. Operating area for HIWC RADAR I (red outline) Flight Information Regions indicated by white lines. Ring radii: green 500 Nm, yellow 750 Nm

### Sampling Strategies

The HIWC RADAR flight sampling strategies were similar to the HAIC-HIWC flight campaigns as outlined in Strapp et al. [4]. Generally, flights would be in large convective storms, ideally in MCSs that developed over the ocean, with cloud tops reaching the tropopause and cloud diameters larger than about 100 Nm. In comparison to deep continental convection, oceanic systems are known to have lower likelihood of hail and lightning, and have weaker updraft velocities. The longer lifetimes and larger cloud extent of MCS compared to isolated convection, provided more persistent targets and longer cloud traverse lengths that were useful for the cloud characterization effort. To be consistent with the sampling strategy recommended by the EHWG as outlined in the HIWC Science and Technical Plan, and the HAIC-HIWC sampling, data were collected in level transects at altitudes associated with the following atmospheric temperature intervals:  $-50^{\circ}\pm 5^{\circ}\text{C}$ ,  $-40^{\circ}\pm 5^{\circ}\text{C}$ ,  $-30^{\circ}\pm 5^{\circ}\text{C}$ , and  $-10^{\circ}\pm 5^{\circ}\text{C}$  (See Figure 5).

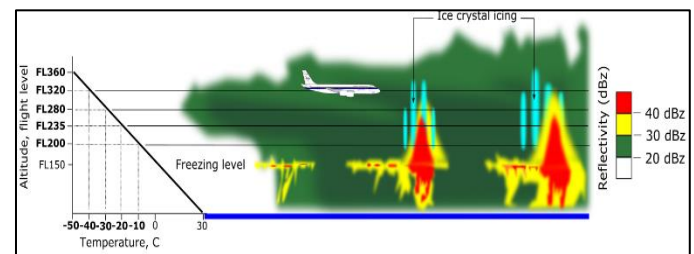


Figure 5. Vertical cross-section schematic of radar reflectivity factor with HIWC RADAR sampling altitudes superimposed

### Concept of Operations

Based on the HAIC-HIWC flight campaign experience, and climatological studies of the southeast Florida operating area, the Science team anticipated convective system life cycles as short as one

<sup>1</sup> TWC is the total condensed water content, equal to the sum of the cloud liquid water and ice water contents.

to two hours. To increase readiness, several teams were formed to perform specific functions. These teams included a Forecast team, Ground Guidance team, Flight team, Instrumentation team, and Science team. Although there were no time of day limitations for performing research flights on the DC-8, a 20-year climatology of satellite-based anvil detections [13] determined that deep convection maximized over the Gulf of Mexico near noon local time. As a result, only daytime operations were anticipated and executed. Table 1 shows the typical daily schedule for a flight duration of five hours.

Table 1 Nominal flight day schedule

Nominal Flight Day Schedule		
Planned Takeoff	8:00	
Planned Flight Time (hr)	5	
Start	End	Times are local EDT time (UTC-4)
4:00	5:00	Forecasting/Nowcasting team preparations
		Launch Ground Crew & Science Team Show Time
5:00	6:00	Weather Team Brief Navigator
5:45		Go/ Delay Decision announced
6:00	6:00	Flight plan filed
6:30	7:00	Crew Brief
7:30	7:30	Flight team onboard; doors closed
8:00		Taxi/Takeoff
8:00	13:00	Ground Team provide updates to DC-8
13:00		Landing
13:30	14:30	Post-flight operations debrief
15:00	17:00	Post-flight review of data / Instrument Post Flight Checks
16:00	17:00	Wx forecast for next day
17:00	17:00	Announcement for start time of next day ops

As can be seen from Table 1, the Forecast team started early in the daily cycle to review weather models, current satellite and radar data, and then prepare the weather brief for the Science team and a DC-8 navigator. Concurrently, the DC-8 ground crew and instrumentation team performed preflight checks. If convective systems were favorable and the aircraft and instruments were “Go”, the flight planning commenced as shown in Table 1. If the weather systems were not developing, the flight was put on “Hold” and the Forecast and Ground Guidance team continued to monitor the weather for other opportunities.

During flight operations, the Ground Guidance team monitored current conditions (Figure 6) and recommended waypoints for the DC-8 to traverse across areas of deep convection (Figure 7), while avoiding areas of intense lightning. The pilots would typically fly along that recommended traverse, but adjusted the course based on radar separation rules (see Mission Rules below). The Flight team reported via a “chat” communication channel to the Ground Guidance team the variations in IWC during the traverse. Subsequent waypoints and flight levels were identified and discussed via chat.

To facilitate the Forecast and Ground Guidance teams, the NASA Langley satellite group developed products specific for the HIWC RADAR campaign [14]. These products utilized GOES-13 data that was updated every 15 minutes. The products were used for pre-flight briefings and uploaded to the DC-8 for onboard decision-making.

After a flight was completed, the whole team debriefed the results from the flight. Subsequently, the Forecast team provided an outlook for the next day, and then the operations plan for the next day was disseminated to the team.

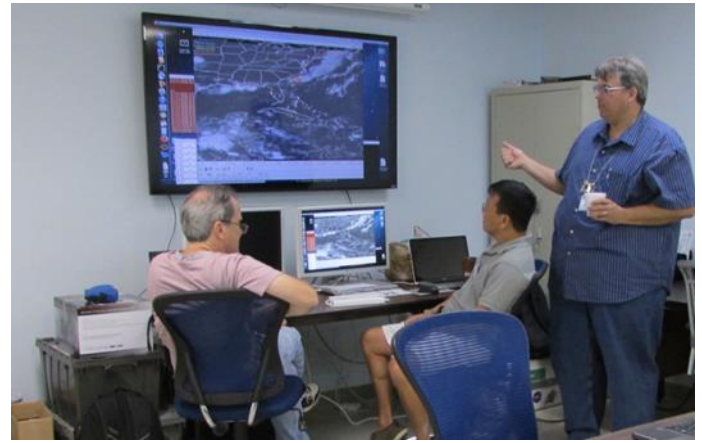


Figure 6. Ground guidance/briefing room at KFL

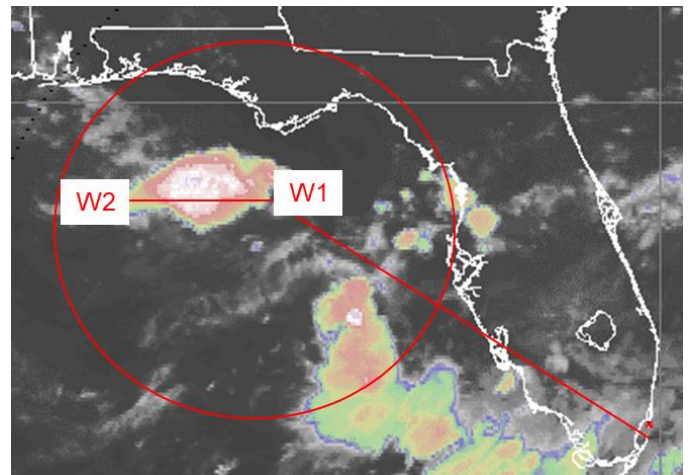


Figure 7. Example of region of interest from IR satellite image with waypoints for first traverse. White areas represent deepest convection with cloud tops near tropopause.

## Mission Rules & Flight Procedures

As part of the campaign planning, NASA Armstrong developed mission rules and procedures to mitigate hazards of flying in and around convective systems. The mission rules included:

- 20 Nm lateral separation from red radar returns (>40 dBZ) at flight level as indicated on the pilots weather radar display. This could be reduced to 10 Nm if the potential for hail was unlikely.
- No flights over red radar returns with less than 5000 ft. of vertical separation.
- 10 Nm lateral separation from yellow radar returns (30-40 dBZ) at flight level as indicated on the pilots weather radar display. This could be reduced provided: 1) no potential for hail, 2) turbulence was less than continuous moderate, and 3) lightning was not a hazard.
- Aircraft commander had the final authority to judge acceptability of the weather conditions.
- Engine igniters were on during icing operations.
- Engine throttles were staggered, and every 5 minutes, the engine powers were cycled to vary engine fan speeds (N1) by 5-10% for 20-30 seconds to shed small amounts of ice that may have built up within the engines.



- If either of the aircraft Indicated Airspeed (IAS) readings was unreliable due to pitot icing, the cloud traverse could be continued at the discretion of aircraft commander.
- If all IAS readings were unreliable, ground speed was monitored. Based on the aircraft commander discretion, the cloud traverse could be continued up to 10 minutes and then conditions exited as soon as practicable.

Go/No-Go criteria included the aircraft Minimum Equipment List (MEL) and research instrumentation such as the Honeywell RDR-4000 CertPort and data systems, IKP2, and PSD probes. The mission rules and Go/No-Go criteria were reviewed prior to each flight.

### Summary of HIWC RADAR I Flights

The NASA DC-8 and test team were on site at KFLI from August 10-30, 2015. In that time, ten research flights were conducted into a variety of deep convective storms over the Atlantic Ocean, Gulf of Mexico, and the Caribbean Sea. Table 2 provides a synopsis of the ten flights including dates, times, locations and types of storms, and notable events. Figure 8 shows the flight tracks for all of the flights. Figure 35 - Figure 44 in the Appendix provide flight tracks and time histories of altitude, temperature and TWC for the research flights made in the 2015 deployment. Time histories are limited to the periods in the clouds of interest. The Infrared (IR) satellite image in these figures is for a nominal time during the in-cloud operation and does not show the progression and decay of the storm during the flight. The storm cloud movement and evolution can be viewed at the NASA Langley satellite website [14]. Note the color scheme in the IR satellite images was adjusted for each flight so that the white-to-pink transition indicated the tropopause temperature for that day. This temperature is indicated on the IR images as “TROPTPINK= XX” in the upper right hand portion of the image. The deepest convection will have cloud top temperatures colder than at the tropopause and is indicated by white and purple color levels.

Table 2. HIWC RADAR I flight summary

HIWC Flt No.	Flight Date	Time (UTC)	Storm Location	Type of Storm	Notable Events
1	8/12/2015	14:28 to 19:46	Atlantic Seaboard	Oceanic MCS	Initial HIWC buildup
2	8/13/2015	14:52 to 19:31	Bahamas	Oceanic MCS	First TAT anomaly
3	8/14/2015	13:01 to 18:40	Bahamas/Gulf of Mexico	Oceanic MCS	TAT anomaly
4	8/16/2015	13:15 to 20:28	Gulf of Mexico	Oceanic MCS	First pitot anomaly
5	8/19/2015	12:06 to 19:27	Louisiana coast	Coastal MCS	Pitot anomaly
6	8/21/2015	13:56 to 21:04	Texas & Louisiana coast	Coastal MCS	No pitot or TAT anomalies
7	8/23/2015	11:20 to 19:41	Eastern Caribbean	Tropical Storm Danny	multiple pitot failures
8	8/26/2015	11:06 to 20:55	Eastern Caribbean	Tropical Storm Erika	multiple pitot failures
9	8/27/2015	12:03 to 22:01	Eastern Caribbean	Tropical Storm Erika	multiple pitot failures
10	8/28/2015	13:20 to 21:07	South of Dominican Republic	Tropical Storm Erika	multiple pitot failures



Figure 8. HIWC RADAR I flight tracks compilation

### Flight 1-6: MCS Examples

HIWC Flight 1 was a “build-up” flight since this was the first intentional flight with the DC-8 into HIWC conditions. This entailed limiting the exposure time to HIWC to confirm acceptable engine performance was met. Flight sampling was conducted at an altitude of 37,000 ft. (-50°C) where IWC was less than 0.1 g m<sup>-3</sup> and at 29,000 ft. (-30°C) where IWC ranged from 0.25 to 1.5 g m<sup>-3</sup> with periods less than 2 minutes where IWC increased up to 2.0 g m<sup>-3</sup>. The radar and icing instruments performed normally and no engine performance issues were observed.

HIWC Flights 1-6 were in MCSs that developed over the Atlantic Ocean and the Gulf of Mexico. These storm systems tended to have smaller areas of deep convection, more lightning, and were in areas of increased air traffic (particularly Flights 5 & 6), all of which adversely affected the data sampling by limiting the traverses that could be taken. The Flight and Ground Guidance teams worked diligently to identify waypoints for data lines that would traverse through areas of deep convection, but provide safe distances from lightning and other hazards. The Ground Guidance team had the benefit of rapid satellite updates, while the Flight team had the benefit of the onboard radar and the stormscope (which provided real-time lightning information). In this way, the flight sampling tracks were adjusted based on the current conditions.

To exemplify some challenges from the first six flights, Figure 9 shows a portion of the Flight 5 flight track overlaid on IR satellite imagery. The white/purple area indicate the coldest tops and deepest convection where the potential for higher concentrations of ice crystals was expected, and generally experienced in the HAIC-HIWC flight campaigns. After the first track on the east side of the storm, the team decided it was better to work on the west side to avoid higher concentrations of lightning and any potential for hail. Air Traffic Control (ATC) was unable to approve a route around the northern edge due to other air traffic. Consequently, the DC-8 flight track skirted around the southern edge of the storm.

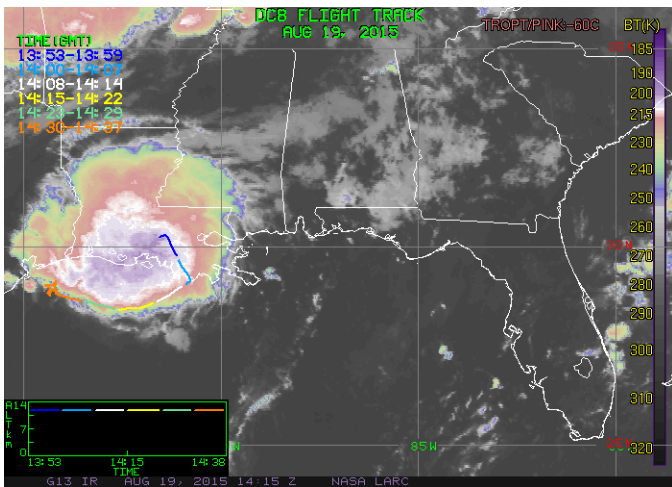


Figure 9. Flight track from Flight 5 with IR satellite. Purple area indicates cold tops and deepest areas of convection

Subsequent flight tracks were altered either due to ATC direction or due to the potential for hail inferred from NOAA NEXRAD ground-based weather radar. Figure 10 illustrates an extended flight track to the north away from the area of interest due to instructions from ATC to allow other traffic to pass through the area. This figure also illustrates the decaying nature of the storm three hours after Figure 9.

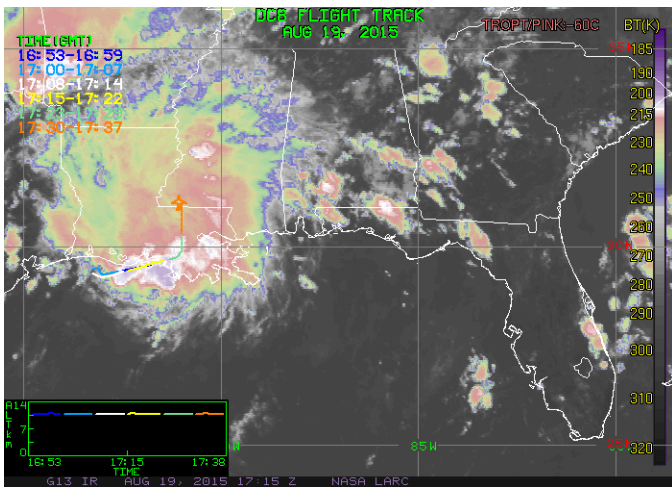


Figure 10. Flight track from Flight 5 with IR satellite. Northerly track extended due to ATC

Another notable characteristic of the storms sampled in these first six flights was the relatively short extent of HIWC regions. Figure 11 illustrates the repeatability of TWC during the course of four parallel tracks at the same altitude during Flight 4 (2015-08-16). As can be seen in Figure 11 as well as Figure 35 - Figure 40 in the Appendix, the duration between the rise and fall of TWC is typically less than 6 minutes, which equates to about 40 Nm in length scale.

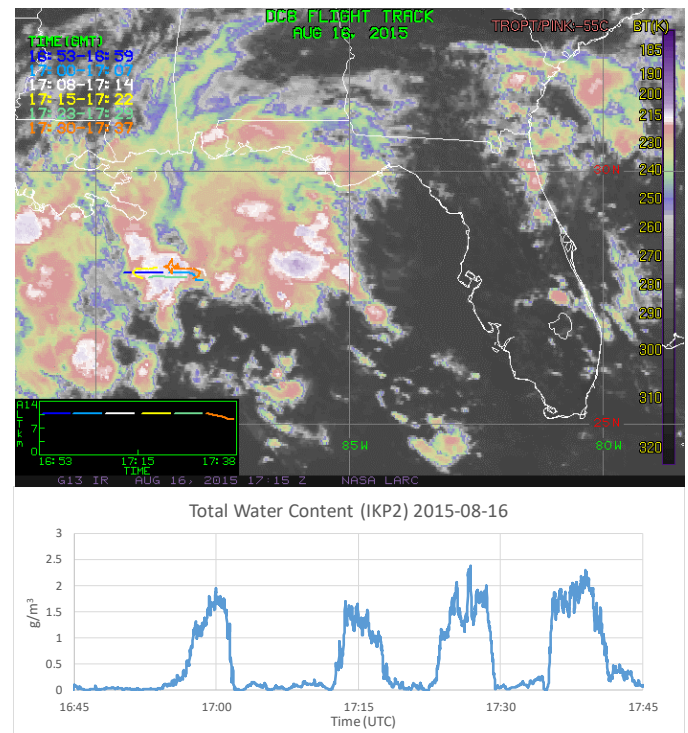


Figure 11. Flight track and total water content time history during four parallel repeat tracks from 2015-08-16

## Flight 7-10: Tropical Storm Examples

During the latter part of the 2015 deployment, tropical systems began to develop off the west coast of Africa, and were monitored by the Forecast team as they moved westward. Although these tropical systems were over 2500 Nm to the southeast of KFL, it was anticipated that they would provide long fetches of HIWC at the desired higher flight altitudes (e.g. -50°C). They also were anticipated to have a lower likelihood of lightning than in some of the previous flights, as well as less ATC restrictions due to being over the ocean. Therefore, after Flight 6 near the Louisiana coast was completed, the team decided to focus on these tropical systems as they tracked westward toward the Caribbean.

HIWC Flights 7-10 (Figure 41 - Figure 44 in the Appendix) were conducted into Tropical Storm Danny and Tropical Storm Erika. As anticipated, these storms provided good HIWC data collection without the need for course deviations due to lightning and/or conflicting air traffic. However, in-cloud course deviations were still often necessary to maintain lateral separation from higher radar reflectivity factor at flight level and to allow iced pitot probes to recover.

As an example of the flights into tropical storms, Figure 12 shows the Flight 10 track overlaid on the IR satellite imagery. The initial waypoint was at the northwest part of the storm and the first data track (shown in light blue) was across the northern side of the storm to an eastern point. The second data track (also shown in light blue) was a back track from east to west with a 10 Nm offset distance to the south of the track 1. As the aircraft approached the western side of the storm during track 2, the pilots deviated to the north to avoid higher reflectivity associated with a significant cell embedded in the tropical storm.

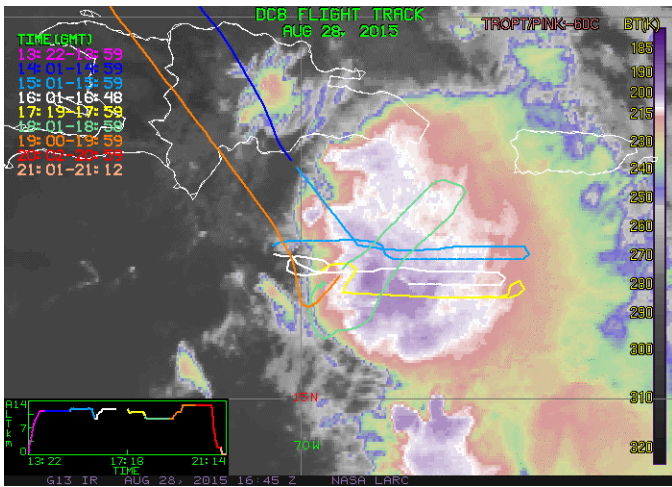


Figure 12. Flight track from Flight 10 with IR satellite (tropical storm Erika) White/purple area indicates cold tops and deepest areas of convection

As anticipated, the tropical storms provided longer exposures to HIWC conditions and the clouds were generally deeper than storms sampled earlier in the campaign, enabling more sampling at higher (colder) altitudes. Figure 13 shows the TWC from tracks 1 and 2 through the northern side of the tropical storm. Note the sharper rise and fall in TWC on the western side (15:10 and 15:52 UTC) and more gradual rise and fall of TWC on the eastern side (15:20 and 15:40 UTC). The storm was tracking westward, so the outflow was generally toward the east. The variation and magnitude of the TWC was remarkably repeatable in these two flight segments. The duration of the TWC “bubble” was about 20 minutes, which equates to about 130 Nm in length scale. The higher TWC during these passes corresponded to the closer proximity of the DC-8 to the higher reflectivity areas displayed on the pilot’s weather radar.

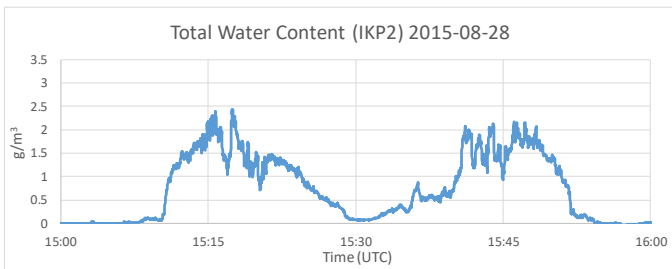


Figure 13. Total Water Content time history during 2 parallel repeat tracks from 2015-08-28

### Pitot Probe Icing

One type of in-service event that has occurred during flights in HIWC conditions is pitot probe icing [15]. During the HIWC RADAR campaign, pitot icing occurred in six of 10 flights. The DC-8 has two pitot probes, one for each air data computer (ADC) to provide airspeed indications to the pilot and copilot. ADC airspeed was also provided to the research data systems to calculate TWC, static temperature, PSD, etc. Consequently, airspeed errors needed to be minimized during the flights and then corrected in post-flight data processing. When pitot anomalies occurred, the flight crew followed the mission rules and monitored alternate sources of airspeed and ground speed, or departed the cloud and descended to clear the pitot probes of icing and restore the airspeed measurements. Figure 14 shows a 15-minute departure to the outside of the western side of cloud and descent to clear the pitot probe icing.

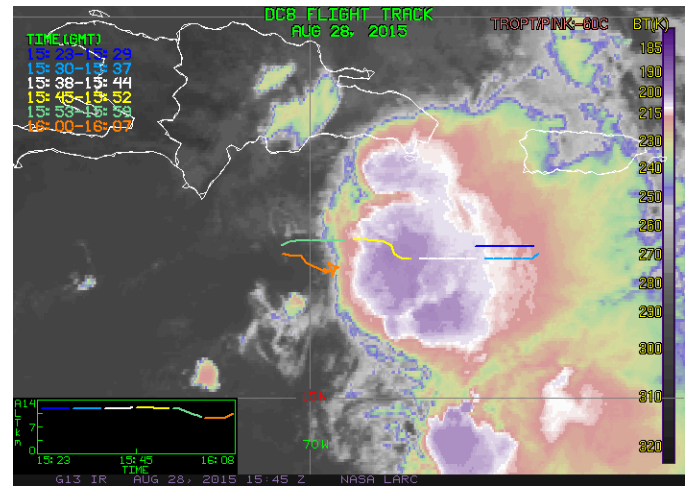


Figure 14. Flight track showing departure from cloud and descent to clear pitot probe icing. Green and orange segments corresponded to flight in clear sky conditions required to clear pitot probe icing.

Two types of airspeed errors were found. In some cases, the pitot probe icing caused abrupt changes to the airspeed. In other cases, the airspeed changed slowly, which was more difficult to detect. Both types were experienced during the first two tracks of Flight 10 and are illustrated in Figure 15. At 15:15 UTC, the airspeed dropped precipitously from 200 m s<sup>-1</sup> to about 80 m s<sup>-1</sup> for a minute, recovered briefly, dropped again for another minute, and then recovered again. At about 15:31 UTC, the airspeed slowly increased, but not so much as to attract attention. Only after the quick drop at about 15:53 UTC was it clear that the airspeed was still unreliable and a descent was initiated to clear the ice blockage from the pitot probes. Post-flight analyses using ground speed, track and prevailing winds were used to correct the time periods when the airspeed was unreliable.

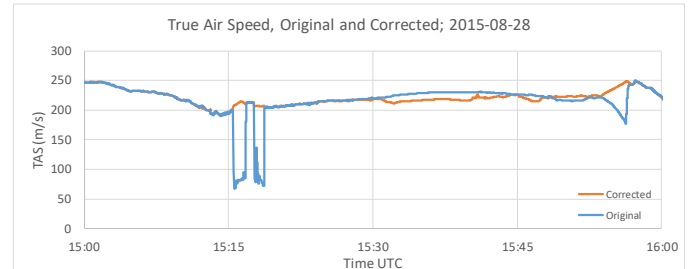


Figure 15. Airspeed anomalies caused by pitot probe icing (2015-08-28)

Figure 16 shows ice that formed on the backside of one of the DC-8 pitot probes after encountering HIWC conditions. This ice formed by ice crystal impinging and melting on the warm pitot probe. The liquid water flowed downstream along the pitot to the colder surface and refroze. Although this ice does not cause the pitot anomaly, it illustrates the melting and re-freezing process that is thought to be occurring inside the pitot probe inlet.



Figure 16. Ice on backside of DC-8 pitot probe after flight in HIWC



## Total Air Temperature (TAT) Probe Icing

Total air temperature (TAT) probe anomalies have also occurred during in-service engine power loss events [16, 2]. Similar to the pitot probe icing, TAT anomalies are thought to result from high concentrations of ice crystals melting and refreezing in the probe inlet, redirecting ice into the sensor cavity, where it accumulates and partially melts near the temperature sensor. The ice-water bath causes the temperature probe to sense a near 0°C reading instead of the TAT. During this flight campaign, a research TAT probe model known to experience in-service TAT anomalies was installed on the DC-8 nose ahead of the windscreen, next to an SEA TWC hot-wire probe measuring the local ice concentrations. Figure 17 shows the ice that formed on the backside of the research TAT probe after flight through HIWC conditions. Figure 18 illustrates the differences in TAT measurements between the research TAT probe and the DC-8 TAT probe. Note how the research TAT rose to near 0°C during the anomalies. The DC-8 TAT probe did not appear to exhibit TAT anomalies during the flight campaign. It was a different TAT probe model and design from the research TAT, and was mounted further forward and on the bottom of the DC-8 nose.



Figure 17. Ice on backside of TAT probe after flight in HIWC

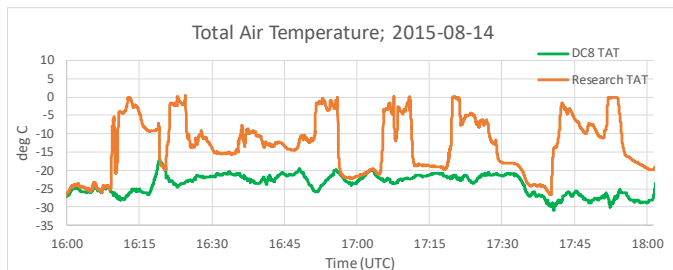


Figure 18. TAT anomalies on Research TAT (2015-08-14)

## Key Findings and Lessons Learned from HIWC RADAR I Flights

Post campaign, the meteorological and radar data sets were processed into quality-controlled data sets of TWC, PSDs, radar reflectivity factor, and other supporting parameters. The processing methods for the TWC have been described in Strapp et al. [9] and Davidson et al. [10]. The PSD processing has been described in Leroy et al. [17]. The radar I&Q data processing is described in Harrah et al. [18]. These data sets were archived by NCAR [19], and made available to the science team for further analyses.

A primary result of HIWC RADAR I was the correlation of radar reflectivity factor to IWC. Figure 19 presents the X-band radar

reflectivity factor measured at the nearest practical range ahead of the airplane vs the IWC measured by the IKP2 for all flights made in the 2015 campaign for static air temperature (SAT) < -15°C. The broad scatter and near vertical segments in the IWC to RRF relationship suggest that reflectivity factor alone is not sufficient to estimate IWC levels since a wide range of IWC are related to a narrow range of RRF. Harrah et al. [18] parsed this data into temperature bins to see if that improved the correlations, but concluded it did not alter the finding significantly, even for radar measurements at close range. Moreover, longer range radar measurements caused larger standard deviations in the correlations, rendering the correlations impractical for operational purposes.

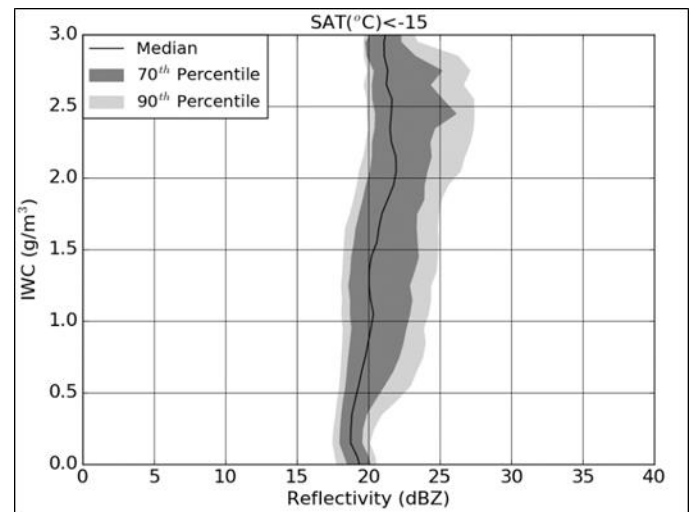


Figure 19. Correlation of RRF to IWC from IKP2 for all 2015 flights and SAT < -15°C [18]

This RRF to IWC correlation data was essential for recommendations made by the EUROCAE WG-95 Long-Range Awareness Subgroup and RTCA SC-230 Working Group 8 in their report entitled, “Feasibility Study: Weather Radar for Ice Crystal Detection” [20]. The group concluded that current airborne weather radar systems do not have sufficient performance to meet the operational targets defined by the aircraft manufacturers. This conclusion was based on the radar reflectivity factor and temperature data available to current airborne weather radar systems. This finding compelled NASA radar researchers to look for other methods to identify HIWC at long ranges, and led to the HIWC RADAR II flight campaign.

Another key result was the contribution of TWC and particle size data, particularly at the -50°C flight level, for an ongoing assessment of the Part 33 Appendix D and corresponding European Aviation and Safety Agency (EASA) CS-25 Appendix P. The results of the assessment are summarized in Strapp et al. [21], an FAA Technical Report to be published in 2019. IKP2 TWC data from deep convective clouds sampled in the 2014 and 2015 HAIC-HIWC flight campaigns and the first HIWC RADAR campaign were combined to provide maximum and 99th percentile TWC values as a function of distance scale. Additionally, particle size data from the three flight campaigns were combined to provide PSD and mass size distributions (MSD), and median mass diameters in HIWC conditions, using techniques described in Leroy et al. [6]. The first HIWC RADAR campaign provided the majority of the data at -50°C, which was considered the highest priority temperature interval for the assessment.

Numerical weather modelling of several of the 2015 data sets was also conducted. Numerical modeling is useful for: 1) model validation, 2)



providing detail and understanding to the characterization of HIWC events, and 3) providing high-resolution data sets containing wind-fields, radar reflectivity factor, and temperature, as well as, cloud, precipitation, and ice fields that can be used to refine HIWC detection and warning systems.

Results from modeling the MCS encountered in Flight 5 were presented by Proctor, et al. [22]. The numerical simulation showed that large volumes of ice crystals can be percolated into the upper-troposphere by regenerating convective plumes associated with a long-lasting MCS. Cloud material carried by the upper-level outflow from these plumes merge to form a large overhanging canopy that contain large areas of HIWC. Large concentrations of ice crystals accumulate over time due to the duration of the system and the presence of weak environmental wind shear. HIWC conditions developed in spite of the updrafts being unsteady, non-adiabatic, and transitory. The model simulations also confirmed that HIWC can occur with low values of radar reflectivity factor due to the large number of small ice particles. The highest concentrations of ice water were located between 20,000 ft-35,000 ft., within and downshear of updraft plumes.

Many of the pilot observations from in-service events [2] and research flights [23] were also confirmed during this campaign. Specifically, there were a number of encounters when IWC exceeded  $1 \text{ g m}^{-3}$  with radar reflectivity factor less than 30 dBZ (black or green displayed on the pilot radar). The DC-8 pilots observed “streaming water” on the windscreen under certain HIWC conditions. Moreover, as shown above, both TAT and pitot anomalies were experienced when the probes were subjected to specific IWC and temperature conditions. More detailed studies on these events are needed to understand threshold conditions that trigger the anomalies, and the localized flowfield and particle concentration effects.

This flight campaign provided lessons-learned which were implemented in the follow-on campaign. As discussed above, the occurrence of pitot probe icing can cause operational and research data issues that require exiting the icing cloud to restore the measurement and the need for substantial post-flight airspeed corrections. This led to a requirement for an “auxiliary” pitot probe with higher deicing heat to be installed prior to a second campaign. Other icing instrumentation issues found during the campaign included significant lags in the background humidity system, occasional fogging of the PIP and CDP-2 optical windows, stuck diodes and at times frequent image buffer decompression issues on the PIP. Most of these were managed in post-processing, but the corrections were labor and time intensive. The takeaway was to add further instrumentation and procedures to mitigate these issues in the second campaign.

Lastly, the operational lessons-learned included the value of tropical storms in providing persistent sources of high IWC, and the importance of the DC-8’s range in reaching such storms at significant distances from a base of operation. Tropical Storms Danny and Erika provided data at longer distance scales and colder temperatures than any of the MCSs that were flown in the first campaign. The tropical storms also had less lightning and hail threats, and less air traffic, which enabled fewer diversions from planned flight tracks. Another valuable lesson was that the DC-8 engines were able to safely operate in the HIWC conditions encountered when using the mission rules and mitigation procedures.

## HIWC RADAR II (2018)

As stated in the previous section, radar data and cloud in-situ data from HIWC RADAR I (2015) campaign were analyzed to determine that RRF alone was insufficient to identify regions of HIWC ahead of the aircraft. However, as a result of the analysis, several radar techniques

were considered to be promising candidates for further research. These techniques included multi-frequency radar, dual-polarimetric (hereafter dual-pol) radar, and a new NASA-developed process called “Swerling” that related the index of dispersion ( $I_D$ ) in X-band radar reflectivity factor to IWC [18]. As discussed in Harrah, et al., the name “Swerling” pays homage to Peter Swerling, a radar theoretician from the 1950’s who developed statistically “fluctuating target” scattering models, but the HIWC discrimination process is very different from his statistical target detection models. The Swerling process was a leading candidate based on test cases from the HIWC RADAR I, and was recognized as an easier retrofit to the current transport aircraft fleet.

A second flight campaign was planned to evaluate the HIWC detection performance of dual-pol radar, the Swerling process, and other radar processes as means for tactical avoidance and decision-making. However, due to hardware delivery issues, the dual-pol capability was not available by the start of the flight campaign. Although this resulted in a shortfall in objectives, the FAA and NASA team decided to continue the flight campaign in order to evaluate the new “Swerling” process in HIWC conditions. A secondary goal of the campaign was to collect additional cloud in-situ measurements in HIWC conditions to compare to data collected in previous flight campaigns.

## NASA DC-8 with HIWC Improved Instrumentation

The NASA DC-8 was used again for this campaign and was similarly instrumented as in the HIWC RADAR I campaign (see instruments section above). However, based on the lessons-learned in the previous campaign, improvements were made to mitigate pitot anomalies, lags in background humidity, and fogging of particle probe optics. Additional instruments were added to obtain wind and turbulence measurements, and localized TWC measurements at the wing pylon and off-fuselage stations. Each of these is described briefly below.

### Auxiliary Pitot-Static Probe

A Rosemount 856DE-6 pitot-static probe with approximately 450 W of anti-icing heat was mounted to the right side fuselage at station 100 (Figure 20). This pitot-static probe was previously tested at National Research Council Canada (NRC) M-7 Test Cell 5 in IWC up to  $9 \text{ g m}^{-3}$  at  $-17^\circ\text{C}$  and  $150 \text{ m s}^{-1}$  with no pitot anomaly. The standard DC-8 pitot probes have approximately 250 W of anti-icing heat, so the extra 200 W of heat was expected to keep this auxiliary pitot probe from failing in HIWC conditions. The pitot inlet was 5” off of the fuselage surface. Data from the auxiliary pitot-static probe was compared to those from the DC-8 ship pitot-static systems during the instrument checkout flight to develop an airspeed correlation for the former. Unfortunately, during flight in HIWC conditions, the auxiliary pitot probe accumulated melted water, which subsequently froze and caused pitot anomalies. Once this was recognized, the data from this probe was not used as a backup to the DC-8 pitot system.



Figure 20. Auxiliary pitot probe installed on DC-8. Inset shows close up.

## Background Humidity Measurement

Since the IKP2 measures water vapor from the ambient air plus the water vapor from evaporated cloud particles, an accurate and responsive measurement of the background humidity is needed to calculate the TWC contained in the evaporated particles. In 2018, several improvements were made to the background humidity system (BHS) used in 2015, and additional background humidity systems were installed. First, the flowpath of the BHS used in 2015 was updated to reduce time lags, and a SpectraSensor Water Vapor Sensing System (WVSS-II) was added in 2018 as a supplementary sensor in-line with the Licor LI840A. Several inlet options for this BHS were mounted on the window blank at station 530 (Figure 21). During initial flights in 2018, the BHS was connected to each of these inlets, and after examining these data sets, the aft facing inlet made from 1/2" OD tubing with a flare at the end (about 10 o'clock position on Figure 21) was determined to be the best option and used thereafter. Unfortunately, even with these improved inlets, the background humidity values appeared to be elevated during HIWC encounters. This indicated ice crystals were ingested into the aft facing tubes, as previously reported by Strapp et al. [9] for similar HAIC-HIWC Falcon-20 humidity observations.

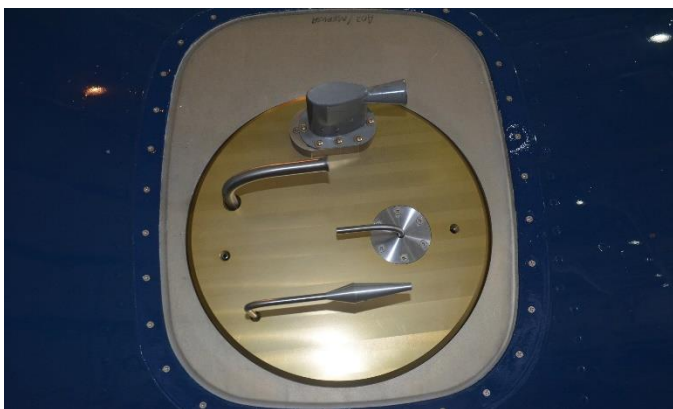


Figure 21. BHS Inlets and solid wire TAT on window blank (station 530)

A second BHS was added to the IKP2 probe itself in 2018. This enabled the background humidity to be measured at the same location as the IKP2 TWC measurement to minimize IKP2 calculation errors and noise caused by phase lag and spatial differences of the IKP2 and background measurements (Strapp et al. [9]). In order to make two water vapor measurements within the IKP2, a customized dual Licor LI-850 system was developed by SEA to replace the single LI840A that had been used in the IKP2 previously. One of the LI-850 units measured the water vapor within the IKP2 flow path (cloud TWC +

background humidity), while the second LI-850 unit measured the background humidity through a small aft facing inlet on the side of the IKP2 canister (Figure 22). Review of the background humidity data from this source found it also had periods of elevated humidity during HIWC encounters, indicating ice crystals contaminated the inlet.



Figure 22. IKP2 canister with inlet for background humidity circled in red

Lastly, the NASA Langley Diode Laser Hygrometer (DLH) [24, 25] was installed on the DC-8 to measure background humidity. The DLH utilizes an open-path, double-pass configuration, where the path is defined on one end by a laser transceiver mounted in the cabin on a modified window blank, and on the other end by a panel of retro-reflecting material mounted on the DC-8's outboard engine nacelle. The DLH is thus not subject to inlet contamination by ice crystals as described above. The DLH proved to be an excellent addition to the HIWC RADAR II instrument suite, and the best source of background humidity for the IKP2 TWC calculations.

## N<sub>2</sub> Purge System for Preventing Particle Probe Optics Fogging, and for BHS Zero

N<sub>2</sub> tanks were installed in the DC-8 cabin and connected to the purge lines that run through the wings to each wing tip pylon. After the completion of a flight, a set of tubing was connected to the wing pylon purge line so that dry N<sub>2</sub> would flow through the PIP and 2D-S probes on the right wing (Figure 23) and to the CDP-2 probe head/canister and the IKP2 flow path and background humidity inlet on the left wing (Figure 24). During preflight checks, the purge lines were removed and the canisters quickly sealed. This procedure was effective at preventing moist air from entering the canister and then condensing inside the canister and optic windows during the flight in subfreezing temperatures. The N<sub>2</sub> tanks were also connected to the rack mounted BHS in order to periodically provide zero humidity air for water vapor instrument calibrations and to purge the inlet lines to keep them dry, for example during descent from high altitude when condensation on cold-soaked inlet lines might be expected.



Figure 23. PIP and 2D-S with purge lines installed on tail cones



Figure 24. IKP2 and CDP-2 probe with purge lines installed

### Meteorological Measurement System (MMS) for Winds and Turbulence

The MMS [26, 27] was installed on the NASA DC-8 to provide high resolution and accurate meteorological parameters (pressure, temperature, turbulence index, and the 3-dimensional wind vector). The MMS consists of three major systems: (1) an air motion sensing system to measure the air velocity with respect to the aircraft, (2) an aircraft motion sensing system to measure the aircraft velocity with respect to the earth, and (3) a data acquisition system to sample, process and record the measured quantities. The MMS has supported many DC-8 missions during the past 20 years and was a very valuable addition to the HIWC RADAR II measurements. It not only provided 3D winds as originally intended, but it also provided the best source of airspeed and static temperature that was used in subsequent data analyses. The MMS pitot probe is uniquely integrated into a Total Air Temperature probe that was mounted on the lower nose of the DC-8 for this mission (Figure 25). Although the DC-8 pitot probes and the auxiliary pitot-static probe suffered numerous pitot anomalies during the 2018 campaign, the MMS airspeed was not significantly affected by the HIWC conditions encountered.



Figure 25. MMS Pitot (left) and TAT probe (right)

### TWC Measurements at Off-Fuselage Locations

As part of an effort to understand TWC location variations, particularly for fuselage mounted probes, another two SEA hot-wire TWC probes were added to the instrument suite. One was located on the CDP-2 canister (left wing pylon- Figure 26) , considered to be close to a free-stream location, while a second was mounted on a window-mounted pylon at station 330 on the left side of the fuselage (Figure 27). Both locations accommodated either an SEA Robust probe [23, 28] or an Ice Crystal Detector probe [29]. Analysis of these measurements, along with the SEA TWC probe on the fuselage nose, will facilitate a better understanding of the ice concentration variation due to localized effects.



Figure 26. CDP-2 canister with SEA Ice Crystal Detector circled in red



Figure 27. SEA Ice Crystal Detector on window-mounted pylon (station 530)

### Optical Ice Detector

The Collins Aerospace Optical Ice Detector (OID), a compact, short-range cloud LIDAR [30, 31], was installed on the DC-8 Airborne Science Laboratory to supply additional cloud water content measurements. The OID transmitted and received light through an optical viewport installed in a window blank at station 290, and sampled the airstream up to 10 meters outside the aircraft. The use of circularly-polarized pulses of laser light allows the OID to determine cloud density and cloud phase, providing estimates of LWC, IWC, and TWC.

### 2018 Campaign Planning and Operations

The campaign plans were nearly identical to the 2015 campaign. The base of operation was Ft. Lauderdale, FL. The campaign duration was 21 days in August 2018 with 50 flight-hours for research. The operating area was the same as 2015 as shown in Figure 4. The concept of operations and the mission rules were also the same as 2015.



## Sampling Strategies

The sampling strategy was consistent with 2015 in terms of the sampling altitudes ( $-50^{\circ}\text{C}\pm 5^{\circ}\text{C}$ ,  $-40^{\circ}\text{C}\pm 5^{\circ}\text{C}$ ,  $-30^{\circ}\text{C}\pm 5^{\circ}\text{C}$  and  $-10^{\circ}\text{C}\pm 5^{\circ}\text{C}$ ), but with an added interest to fly also at  $-25^{\circ}\text{C}\pm 5^{\circ}\text{C}$  levels when mission rules allowed. Based on adiabatic estimates of maximum condensed water that are the basis of the Appendix D TWC envelope [1], and numerical simulation results by Protor, et al. [22], there was reason to believe that TWC values might maximize in the  $-20^{\circ}$  to  $-30^{\circ}\text{C}$  temperature interval. This flight level was not identified as a priority by the EHWG, and was not a focus for the HAIC-HIWC and first HIWC RADAR campaigns.

As in 2015, the regions of interest were identified by the Forecast team for preflight planning and then adjusted per Ground Guidance team using the products developed by the NASA Langley satellite group [32]. For the 2018 campaign, these products used GOES-16, which had a 2-3 km resolution and was normally updated every 15 minutes, and on special request to NOAA, was updated every 1 minute or 5 minutes. The increased temporal sampling and reduced time latency of the GOES-16 satellite imagery increased situational awareness to optimize the in-cloud sampling.

Additionally, as the flight team gained experience with the Radar identified IWC (R-IWC) levels defined by the Swerling process, the sampling strategy transitioned from point-to-point level transects to tracks that were modified in real-time to intercept areas of HIWC that were detected ahead by the radar.

## Summary of HIWC RADAR II Flights

The instrument upload took place at NASA Armstrong's Palmdale facility in July 2018 and instrument test flights were conducted from there as well. The DC-8 and research teams arrived at KFLI on July 30. The operations base was set up and the Forecast team monitored conditions.

Table 3 provides a synopsis of the ten flights including dates, times, locations, types of storms, and notable events. Figure 45 to Figure 51 in the Appendix provide quick looks for the seven 2018 research flights, including flight track and time histories of altitude, temperature, updraft velocity, and TWC. Time histories are limited to the periods in the clouds of interest. As with the 2015 figures, the IR satellite image in these figures is for a nominal time during the in-cloud operation, so it does not show the progression and decay of the storm during the flight.

Table 3. HIWC RADAR II flight summary

HIWC Flt No.	Flight Date	Time (UTC)	Storm Location	Type of Storm	Notable Events
1	7/27/2018	20:05 to 23:10	NA		Instrument Check Fit
2	7/30/2018	16:04 to 20:52	NA		Ferry to KFLI
3	8/2/2018	14:07 to 19:02	Gulf of Mexico	Oceanic MCS	TAT anomaly
4	8/6/2018	11:31 to 16:36	Gulf of Mexico	Oceanic MCS	TAT anomaly, Aux pitot anomaly
5	8/8/2018	14:25 to 18:52	NA		Ferry to KPMD; #4 engine oil leak
6	8/15/2018	15:19 to 01:23*	eastern Pacific	Tropical Depression 14-E	TAT anomaly, ADC and Aux pitot anomalies
7	8/16/2018	16:22 to 02:30*	eastern Pacific	Tropical Storm Lane	TAT anomaly, Aux pitot anomaly
8	8/18/2018	14:57 to 22:41	eastern Pacific	Hurricane Lane	TAT anomaly, Aux pitot anomaly
9	8/19/2018	17:20 to 00:13*	eastern Pacific	Hurricane Lane	TAT anomaly, Aux pitot anomaly
10	8/20/2018	17:57 to 03:09*	eastern Pacific	Hurricane Lane	TAT anomaly, Aux pitot anomaly

\* denotes next day

## Plans vs Actual

Two research flights were made into MCS within the Gulf of Mexico on Aug-02 and Aug-06 (Figure 28). These storms tended to be shallower, smaller scale, and shorter lived than anticipated for typical HIWC systems. The Forecast team noted that dry air and dust coming from Africa and cooler ocean temperatures in the Caribbean were suppressing the development of deep convection systems. Meanwhile, multiple MCS, tropical storms, and hurricanes were developing in the eastern Pacific off the Mexican coast.

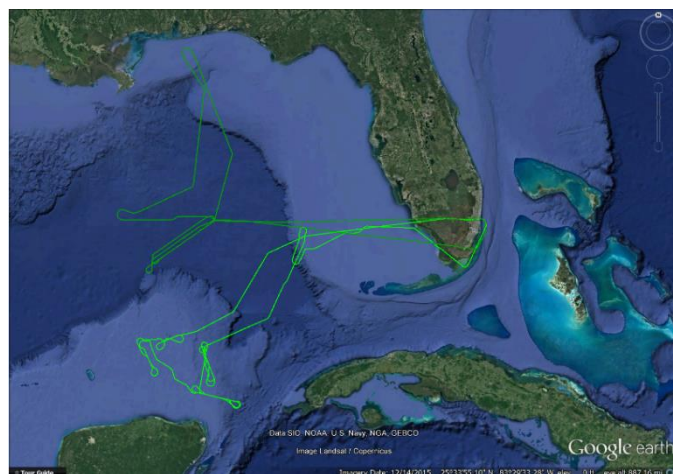


Figure 28. Flight tracks for Flight 03 (central gulf) and Flight 04 (near Yucatan peninsula)

After completing the Aug-06 flight, the team decided to move the base of operations back to NASA Armstrong's Palmdale facility to fly into the convective systems occurring in the eastern Pacific. During the ferry flight back to Palmdale, a significant engine oil leak developed, requiring replacement of the #4 engine. The AFRC crew worked quickly to remove and replace the engine, perform ground checks, and then replace another component within 5 working days.

When continuation of flight operations was approved, five flights were made over the eastern Pacific to acquire data in Tropical Depression 14-E, and subsequently as it developed into Tropical Storm and Hurricane Lane (Figure 29). As the hurricane moved westward, it was determined that more time could be spent in the system if the base of operations was moved to Kona, Hawaii. Consequently, the last three flights had Kona as an arrival and/or departure location.

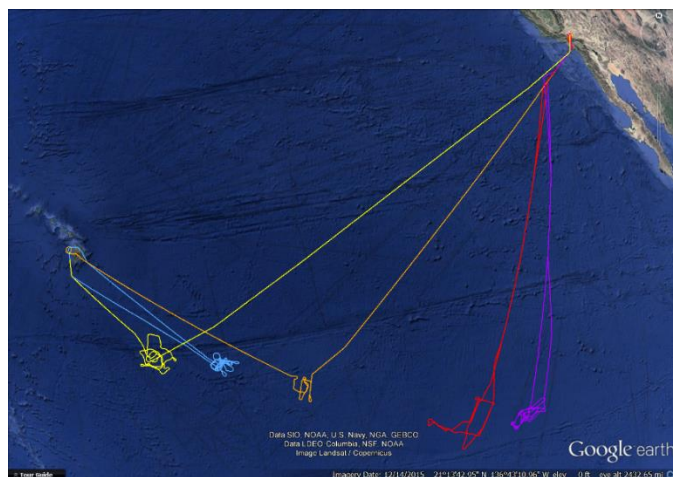


Figure 29. Flight tracks for Flights 06-10

## A Closer Look at Flight 7: Tropical Storm Lane

After a successful, but long 10.1 hour flight on Aug-15 into Tropical Depression 14-E, the forecast team continued to watch the system as it moved westward. The Aug-16 14:00 UTC weather brief indicated that Tropical Depression 14-E had intensified into Tropical Storm Lane and was the best target for HIWC research that day. The storm was approximately 300 Nm in diameter and had large regions of embedded deep cloud (Figure 30).

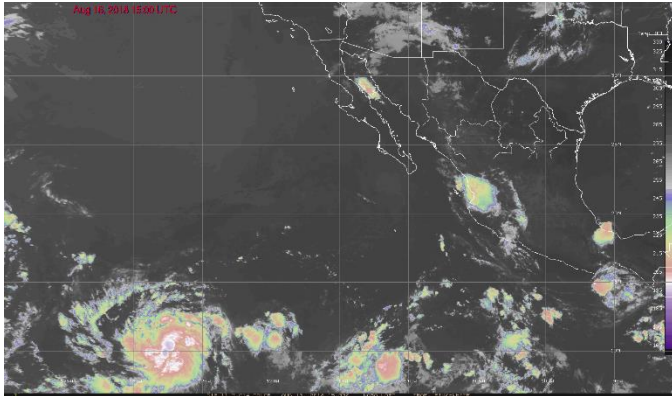


Figure 30. IR Satellite image at 15:00 UTC on Aug-16, 2018 (1 hour before takeoff)

The DC-8 took off at 16:22 UTC and arrived at the outer bands on the northeast edge of Tropical Storm Lane at 19:16 UTC. During the transit, some of the deeper clouds in the outer bands decayed, but the central deep cloud remained, and new deep convective cells were forming into distinct bands. The first transect was made at an altitude of 34,000 ft. and SAT of  $-39^{\circ}\text{C}$  through the deep clouds as shown in Figure 31. The magnitude of IWC during this track was relatively moderate with peaks up to about  $1.5 \text{ g m}^{-3}$ . These deeper cloud regions were in a decaying phase.

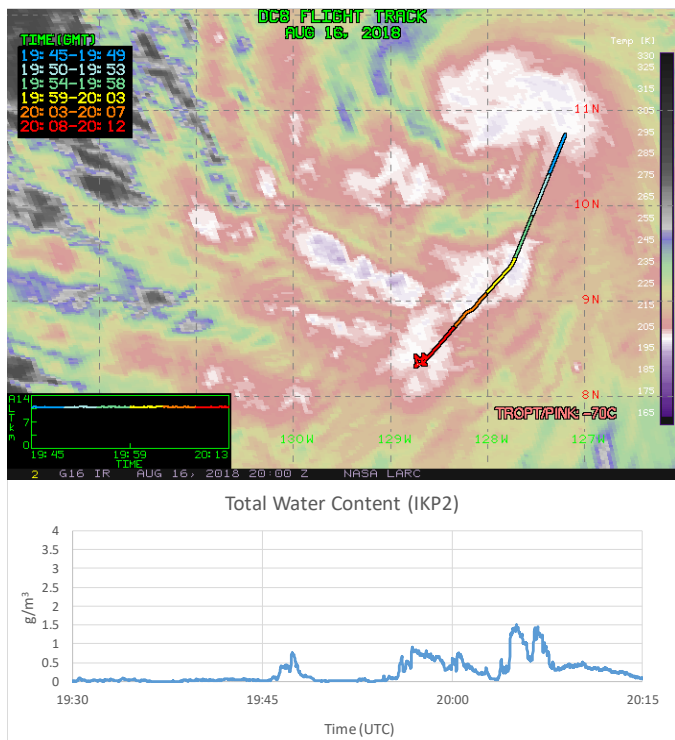


Figure 31. Flight track on IR Satellite image from 20:00 UTC and IKP2 TWC time history on Aug-16, 2018

The next track turned north to return to the larger deep region nearly 200 Nm away at the north side of the storm. On the way, the Radar flight team requested a slight left turn to intercept a cloud region that the Swerling process' Radar Ice Water Content (R-IWC) indicated was approximately  $2.5 \text{ g m}^{-3}$ . Figure 32 shows the DC-8 left deviation to intercept the eastern edge of a developing deep band (black circled region). At 20:28 UTC, a peak TWC of nearly  $2 \text{ g m}^{-3}$  was measured by the IKP2 during this intercept. This level of agreement between the R-IWC and IKP2 TWC was also observed in previous flights, and this event further increased the team confidence in the R-IWC product.

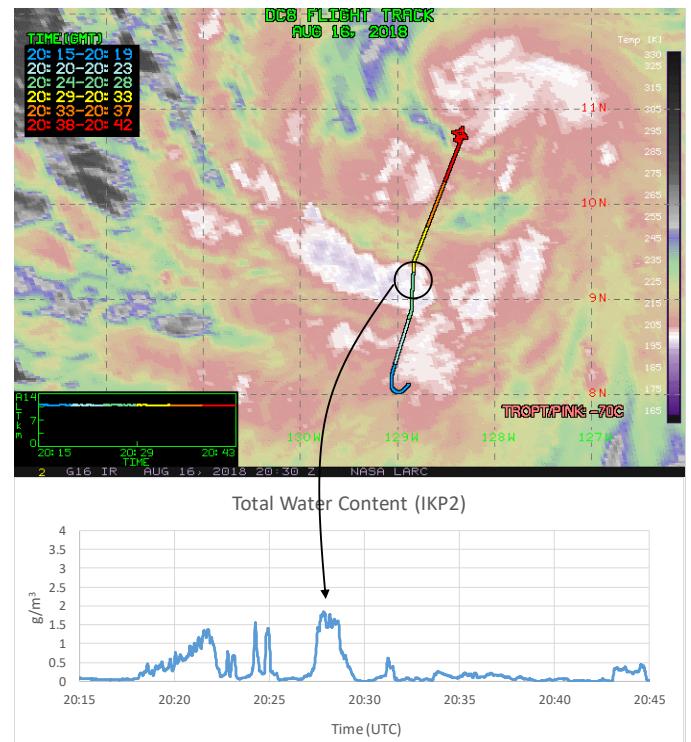


Figure 32. Flight track on IR Satellite image from 20:30 UTC and IKP2 TWC time history on Aug-16, 2018

As the storm transitioned and the areas of deep convection changed rapidly, the remaining flight tracks were guided by the Radar flight team using the onboard R-IWC product and the HIWC Potential Satellite product [33, 34]. These products were displayed in the cockpit, which enabled the pilots to quickly make course changes to intercept the shrinking HIWC regions.

Figure 33 provides an example of flight track deviations made to intercept areas identified by the R-IWC display. This figure also shows a plan position indicator (PPI) display of R-IWC out to 60 Nm ahead of the DC-8 with the flight track color-coded based on the IKP2 binned TWC values. A similar PPI display of R-IWC was presented to the Radar flight team during the flights. The TWC time history in this figure also has the R-IWC values co-plotted with the IKP2 values. The DC-8 position on the PPI is indicated on the TWC time history with a yellow star. As shown on the PPI at 21:37 UTC, there was a region with  $2 \text{ g m}^{-3} < \text{R-IWC} < 3 \text{ g m}^{-3}$  about 50 Nm ahead and to the left of track. Discussion onboard and through the chat, the team decided to make a left deviation to intercept that region. Figure 34 shows the PPI at 30 Nm from the regions of interest. Note the R-IWC values increased to  $2.5\text{--}3.0 \text{ g m}^{-3}$  (cyan color), but the general size of the region was consistent with the R-IWC estimate made from 50 Nm range. Also note the general agreement in IKP2 to R-IWC values in the flight track.



range of the R-IWC Swerling product was approximately 60 Nm as configured for this flight campaign. Harrah et al. [18] have concluded that the range can be extended to 80 Nm or more.

## Key Findings and Lessons Learned from HIWC RADAR II Flights

Meteorological and radar data sets were processed into quality-controlled data sets, although at the time of this publication, some quality control work was ongoing. The IKP2 TWC utilized background humidity from the DLH and static temperature and true airspeed from the MMS using the process described in Strapp et al. [9]. The IKP2 data shown in this report for the 2018 flights is version 1.5. The radar reflectivity factor and R-IWC were derived as described in Harrah et al. [18]. Particle size and mass distributions are being processed by NCAR using methods similar to Leroy et al. [17]. These files will be archived by NCAR [18], and made available to the Science team for reference and further analyses.

The primary objective of the HIWC RADAR II campaign was to acquire data to evaluate and assess the Swerling R-IWC detection method to enable tactical avoidance of regions of potentially hazardous ice crystal icing conditions. Seven flights were made into regions of HIWC conditions that were remotely detected using the R-IWC product, followed by in-situ measurements of the ice cloud conditions. Real-time estimates of IWC were made up to 60 Nm ahead of the aircraft and then confirmed with the in-situ measurements within  $\pm 0.5 \text{ g m}^{-3}$  in certain cases as described above. Post-flight data from all 2015 and 2018 flights were reprocessed using the same relationship between the index of dispersion ( $I_D$ ) to IWC that was used in real time during the 2018 flights. Analyses are ongoing to identify improvements as described in Harrah, et al. [18].

Data from this campaign can also be used to compare to HIWC characterization data from previous flight campaigns, support satellite and weather forecast tool development, examine ice concentration factors in localized areas of an airplane, and much more.

Several diagnostic products were developed by the NASA Langley satellite group and were very useful for providing strategical and tactical guidance during the HIWC deployments. One diagnostic product provided current probability of HIWC with IWC greater than  $0.5 \text{ g m}^{-3}$  [33]. This product is based on geostationary satellite imagery and was developed from statistical relationships between IWC and satellite-derived parameters. Preliminary assessments produced a 75% Probability of Detection (POD) and 37% False Alarm Rate (FAR). Further evaluation is underway using the HIWC data collected in 2018 [34].

Lessons-learned in this campaign include the value of the DLH in solving a long-standing problem in measuring background water vapor in HIWC conditions to support IKP2 TWC calculations, and the value of the MMS in providing accurate and dependable true airspeed, temperature, and wind measurements in HIWC conditions. As a result, processing time and confidence in IKP2 TWC measurements were improved. The DLH enabled comparisons to previous and new methods for acquiring background humidity using aft facing air inlets. The comparisons showed the inlets of various designs continued to have contamination issues when encountering HIWC conditions.

Lastly, an operational lesson learned was the value of using an aircraft with long-range capability for this type of research, and having a flight and research team that was willing and persistent to adapt to the weather changes and overcome unpredictable obstacles and events.

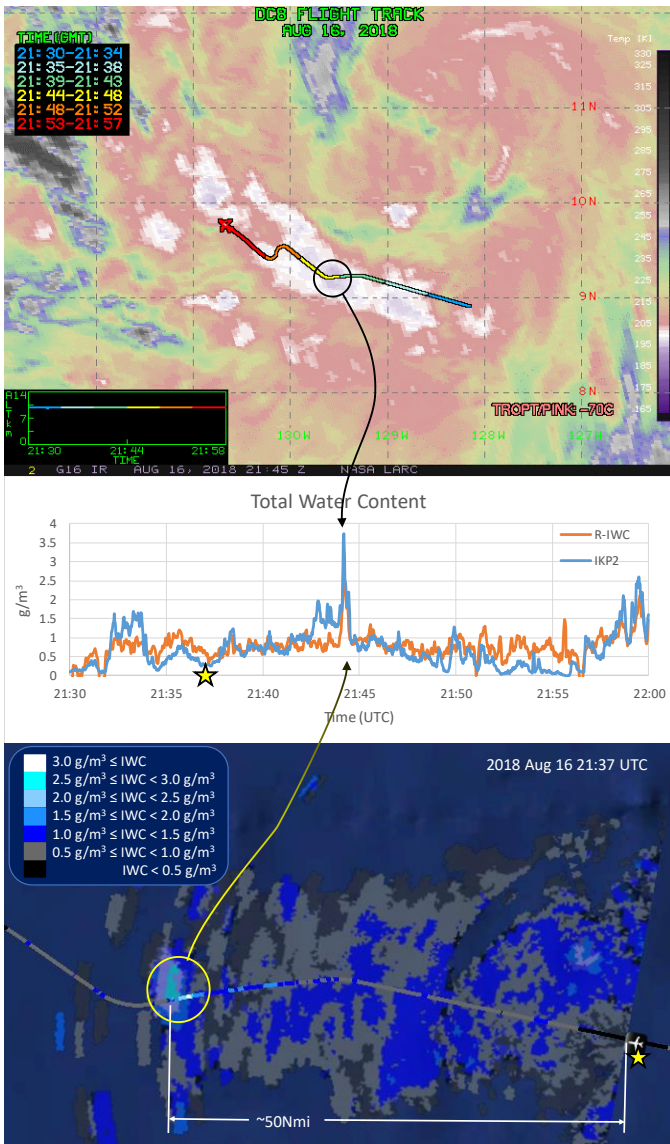


Figure 33. Flight track on IR Satellite image from 21:45 UTC, time history of IKP2 and R-IWC TWC, and PPI of R-IWC display from Aug-16, 2018

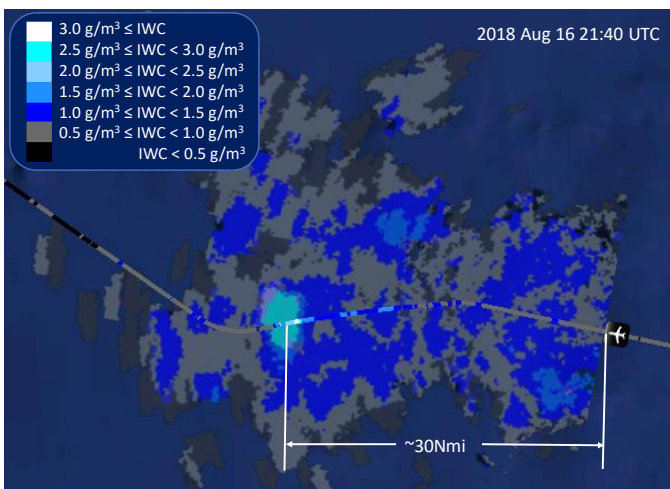


Figure 34. PPI of R-IWC and DC-8 flight track with IKP2 binned values

Flight 7 was a clear transition point when confidence in the Swerling R-IWC product was established, and it was used to guide flight track choices in the remaining flights into Hurricane Lane. The maximum



## Summary/Conclusions

NASA and the FAA conducted two HIWC RADAR flight campaigns to understand and improve radar detection of high ice water content regions ahead of an airplane, and to develop and test new remote detection algorithms that will enable pilots to tactically avoid hazardous regions with high concentrations of ice crystals. The flight campaigns used NASA's DC-8 Airborne Science Laboratory fitted with a Honeywell RDR-4000 radar and cloud in-situ microphysical instruments, specifically modified for HIWC conditions, in order to correlate the radar and HIWC cloud data.

### Key Results and Outcomes from the HIWC RADAR Campaigns:

- Measurements of radar reflectivity factor and particle size distribution confirmed findings and observations by Mason et al. [2], Protat, et al. [8], and Leroy et al. [7], that high concentrations of small ice particles can cause high IWC conditions with low radar reflectivity factor.
- Relationships between X-band radar reflectivity factor and ice water content were developed for various ranges ahead of the aircraft. Even at the closest range, the degree of variability in the measured reflectivity to IWC relationship prevents the RRF alone from meeting commercial operational goals.
- NASA developed a new radar data processing technique called "Swirling" using the HIWC RADAR I data that related the index of dispersion in X-band radar reflectivity to IWC. The Swirling technique was tested during HIWC RADAR II, which identified HIWC regions up to 60 Nm ahead of the airplane [18].
- Cloud characterization data (TWC and particle & mass distributions) from the HIWC RADAR I campaign supplemented HAIC-HIWC flight campaign data requirements, particularly at the -50°C flight level.
- Peak IWC values over distances of approximately 1 km ranged between 1.8 to 3.7 g m<sup>-3</sup> during these flights. Encounters with persistent IWC greater than 1 g m<sup>-3</sup> could last 15-minutes during flight legs in tropical oceanic convective systems. Highest concentrations tended to be near and downstream from active convection with overshooting cloud tops.
- Flight campaign data including onboard weather radar, TWC, PSD, MSD, air data and flight parameters are currently being archived at NCAR [19]. These data are a unique source of validation data for numerical weather models and special forecast and nowcast tools such as the NASA Langley HIWC Potential satellite product [33, 34] and NCAR's Algorithm for the Prediction of HIWC Areas (ALPHA) product [35].

### Lessons learned:

- Tropical systems such as tropical depressions and tropical storms can be efficient and reliable sources of HIWC data. These systems are relatively easy to track, persist for days, have less lightning and hail than continental convection, and produce areas of high ice concentrations over long distance scales.
- The DC-8 proved to be an excellent aircraft for HIWC research due to its range and altitude performance. No engine icing issues were experienced, although pitot probe icing did occur in certain HIWC conditions. The long range and endurance capability of the DC-8 was essential for flights into tropical storms and hurricanes.
- The technical capabilities of GOES-16 increased temporal sampling and reduced time latency. This advancement, coupled with improved satellite products, led to better identification of

storm cell growth and decay that informed flight routing decisions.

- The Diode Laser Hygrometer (DLH) and Meteorological Measurement System (MMS) proved to be very valuable additions to the instrument suite in 2018 in order to obtain accurate background humidity, static air temperature, true airspeed, and winds during these flights into HIWC conditions. Other systems previously used to obtain these parameters were compromised to varying degrees due to ice contamination.

### Future Work/Issues

- The HIWC RADAR data sets are limited to oceanic, northern hemisphere, low-mid latitude storms. Radar-based IWC detection is untested and unknown for other storm types such as continental deep convection, which typically is more vigorous, has higher lightning frequency, and likely contains higher radar reflectivity factor at flight altitude.
- RTCA SC-230 WG-10 has initiated development of Minimum Operational Performance Standards (MOPS) for radar detection of HIWC conditions. Data from these campaigns will provide critical information to this group.
- An Ice Crystal Icing ARAC has been formed to assess the Title 14 Code of Federal Regulations Part 33 Appendix D mixed-phase/glaciated environmental envelope, using flight in-situ data from the Darwin (2014) and Cayenne (2015) HAIC-HIWC flight campaigns, and the first HIWC-RADAR flight campaign [21]. Any gaps in the current data sets identified by this committee may establish the need for additional flight measurements. If so, further testing of onboard pilot radar detection would be beneficial.

## References

1. Mazzawy, R., and Strapp J.W., "Appendix D – An Interim Icing Envelope: High Ice Crystal Concentrations and Glaciated Conditions," 2007 SAE Transactions, *Journal of Aerospace*, 116, 634-642. <https://doi.org/10.4271/2007-01-3311>
2. Mason, J., Strapp, J.W., Chow, P., "The Ice Particle Threat to Engines in Flight," AIAA 2006-0206, 2006, <https://doi.org/10.2514/6.2006-206>
3. "Mixed-Phase/Glaciating Icing Technology Plan," Version 1.1, Engine Harmonization Working Group, December 20, 2005.
4. Strapp, J. W., Isaac, G., Korolev, A., Ratvasky, T., et al., "The High Ice Water Content (HIWC) Study of Deep Convective Clouds: Science and Technical Plan," DOT/FAA/TC-14/31, 2016, <http://www.tc.faa.gov/its/worldpac/techrpt/tc14-31.pdf>.
5. Dezitter, F., Grandin, A., Brenguier, J.-L., Hervy, F., et al., "HAIC – High Altitude Ice Crystals," AIAA 2013-2674, 2013, <https://doi.org/10.2514/6.2013-2674>
6. Leroy, D., Fontaine, E., Schwarzenboeck, A., Strapp, J.W., "Ice Crystal Sizes in High Ice Water Content Clouds. Part I: On the Computation of Median Mass Diameter from In Situ Measurements," *J. Atmos. Ocean. Technol.*, 33, 2461–2476, 2016, <https://doi.org/10.1175/jtech-d-15-0151.1>
7. Leroy, D., Fontaine, E., Schwarzenboeck, A., Strapp, J.W., et al., "Ice Crystal Sizes in High Ice Water Content Clouds. Part II: Statistics of Mass Diameter Percentiles in Tropical Convection Observed during the HAIC/HIWC Project," *J. Atmos. Ocean. Technol.*, 34, 117–136, 2017, <https://doi.org/10.1175/jtech-d-15-0246.1>
8. Protat, A., Delanoë, J., Strapp, J.W., Fontaine, E., et al., "The Measured Relationship between Ice Water Content and Cloud Radar Reflectivity in Tropical Convective Clouds," *J. Appl.*

- Meteor. Climatol.*, 55, 1707–1729, 2016, <https://doi.org/10.1175/jamc-d-15-0248.1>
9. Strapp, J.W., Lilie, L., Ratvasky, T., Davison, C., et al, “Isokinetic TWC Evaporator Probe: Development of the IKP2 and Performance Testing for the HAIC-HIWC Darwin 2014 and Cayenne Field Campaigns,” 8th AIAA Atmospheric and Space Environments Conference, AIAA Aviation, AIAA 2016-4059, 2016, <http://dx.doi.org/10.2514/6.2016-4059>
  10. Davidson, C., Strapp, J.W., Lilie, L., Ratvasky, T., et al, “Isokinetic TWC Evaporator Probe: Calculations and Systemic Uncertainty Analysis,” 8th AIAA Atmospheric and Space Environments Conference, AIAA Aviation, AIAA 2016-4060, 2016, <http://dx.doi.org/10.2514/6.2016-4060>
  11. Korolev, A., Emery, E., Creelman, K., “Modification and Tests of Particle Probe Tips to Mitigate Effects of Ice Shattering,” *J. Atmos. Oceanic Technol.*, 30, 690–708, 2013, <https://doi.org/10.1175/JTECH-D-12-00142.1>
  12. Korolev, A., Emery, E., Strapp, J.W., Cober, S., et al., “Small Ice Particles in Tropospheric Clouds: Fact or Artifact?” Airborne Icing Instrumentation Evaluation Experiment. *Bull. Amer. Met. Soc.*, 92, 967-973, 2011, <https://doi.org/10.1175/2010bams3141.1>
  13. Bedka, K., Khlopenkov, K., “A Probabilistic Pattern Recognition Method for Detection of Overshooting Cloud Tops Using Satellite Imager Data,” *J. Appl. Meteor. Climatol.*, 55, 1983–2005, <http://doi.org/10.1175/jamc-d-15-0249.1>
  14. NASA, “Langley Satellite Support for HIWC RADAR (2015) Campaign”, <https://cloudsway2.larc.nasa.gov/cgi-bin/site/showdoc?docid=4&cmd=field-experiment-homepage&exp=HIWC-PR-2015>, accessed Feb. 2019.
  15. Duviver, E., “High Altitude Icing Environment,” Intl. Air Safety and Climate Change Conf., 8-9 Sep. 2010, Cologne, Germany. [https://www.easa.europa.eu/conferences/iascc/doc/Workshop%201%20Presentations/Workshop1\\_DAY%202/1\\_Duvivier\\_EAS\\_A/IASCC\\_E%20Duvivier.pdf](https://www.easa.europa.eu/conferences/iascc/doc/Workshop%201%20Presentations/Workshop1_DAY%202/1_Duvivier_EAS_A/IASCC_E%20Duvivier.pdf)
  16. Lawson, R.P., Angus, L.J., and Heymsfield, A.J., “Cloud Particle Measurements in Thunderstorm anvils and Possible Threat to Aviation,” *J. Aircraft*, Vol. 35, No. 1, 1998, pp. 113-121. <https://doi.org/10.2514/2.2268>
  17. Leroy, D., Fontaine, E., Schwarzenboeck, A., Strapp, J.W., “Ice Crystal Sizes in High Ice Water Content Clouds. Part I: On the Computation of Median Mass Diameters from In Situ Measurements,” *J. Atmos. Oceanic Technol.*, 33, 2461–2476, 2016, doi: <https://doi.org/10.1175/JTECH-D-15-0151.1>
  18. Harrah, S., Strickland, J., Hunt, P., Proctor, F., et al, “Radar Detection of High Concentrations of Ice Particles – Methodology and Preliminary Flight Test Results,” SAE Technical Paper 2019-01-2028, 2019.
  19. NCAR Archives; “HIWC-RADAR Study”, <https://data.eol.ucar.edu/project/HIWC-RADAR> and <http://data.eol.ucar.edu/project/HIWC-RADAR-2018>, accessed Feb. 2019
  20. “Feasibility Study: Weather Radar for Ice Crystal Detection,” EUROCAE WG-95 Long-Range Awareness Subgroup and RTCA SC-230 Working Group 8, February 2017.
  21. Strapp, J.W., Schwarzenboeck, A., Bedka, K., Bond, T., et al., “An Assessment of Cloud Total Water Content and Particle Size from Flight Test Campaign Measurements in High Ice Water Content, Mixed Phase/Ice Crystal Icing Conditions: Primary In-Situ Measurements,” DOT/FAA/TC-18/1, in publication process
  22. Proctor, F.H., Harrah, S., Switzer, G., Strickland, J., et al., “High Ice Water Concentrations in the 19 August 2015 Coastal Mesoconvective System,” AIAA 2017-4370, 2017, <https://doi.org/10.2514/6.2017-4370>
  23. Grandin, A., Merle, J-M, Weber, M., Strapp, J.W., et al., “AIRBUS Flight Tests in High Total Water Content Regions,” AIAA 2014-2753, 2014, <http://dx.doi.org/10.2514/6.2014-2753>
  24. Diskin, G., Podolske, J., Sachse, G., Slate, T., “Open-Path Airborne Tunable Diode Laser Hygrometer,” Diode Lasers and Applications in Atmospheric Sensing, *SPIE Proceedings 4817*, 196-204, 2002, <https://doi.org/10.1117/12.453736>
  25. NASA Airborne Science Program, Diode Laser Hygrometer (DLH), <https://airbornescience.nasa.gov/instrument/DLH>, accessed Feb. 2019.
  26. NASA, “Meteorological Measurement System” <https://earthscience.arc.nasa.gov/mms>, accessed Feb. 2019
  27. Gaines, S. E., S. W. Bowen, R. S. Hipskind, T.P. Bui, and K. R. Chan, “Comparisons of the NASA ER-2 meteorological measurement system with radar tracking and radiosonde data,” *J. Atmos. Ocean. Tech.*, 9, 210-225, 1992, [https://doi.org/10.1175/1520-0426\(1992\)009%3C0210:cotnem%3E2.0.co;2](https://doi.org/10.1175/1520-0426(1992)009%3C0210:cotnem%3E2.0.co;2)
  28. Strapp, J.W., MacLeod, J., Lilie, L., “Calibration of Ice Water Content in a Wind Tunnel / Engine Test Cell Facility,” 15th Inter. Conf. On Clouds and Precipitation, Cancun, Mexico, 7-11 July 2008.
  29. Lilie, L., Sivo, C., Bouley, D., “Description and Results for a Simple Ice Crystal Detection System for Airborne Applications,” AIAA-2016-4058, 2016, <https://doi.org/10.2514/6.2016-4058>
  30. Ray, M. and Anderson, K., “Analysis of Flight Test Results of the Optical Ice Detector,” *SAE Int. J. Aerosp.* 8(1):1-8, 2015, <https://doi.org/10.4271/2015-01-2106>
  31. Anderson K., Ray, M., “SLD and Ice Crystal Discrimination with the Optical Ice Detector,” SAE Technical Paper 2019-01-1934, 2019.
  32. NASA, “Langley Satellite Support for HIWC RADAR 2018 Campaign”, <https://cloudsway2.larc.nasa.gov/cgi-bin/site/showdoc?docid=4&cmd=field-experiment-homepage&exp=HIWC-2018>, accessed Feb. 2019.
  33. Yost, C. R., Bedka, K. M., Minnis, P., Nguyen, L., et al., “A Prototype Method for Diagnosing High Ice Water Content Probability using Satellite Imager Data,” *Atmos. Meas. Tech.*, 11, 1615-1637, 2018, <https://doi.org/10.5194/amt-11-1615-2018>
  34. Bedka, K., Yost, C., Nguyen, L., Strapp, J.W., et al., “Analysis and Automated Detection of Ice Crystal Icing Conditions Using Geostationary Satellite Datasets and In Situ Ice Water Content Measurements,” SAE Technical Paper 2019-01-1953, 2019.
  35. Rugg, A., Haggerty, J., Ratvasky, T., Strapp, J.W., “Recent Updates to the Algorithm for the Prediction of High Ice Water Content Areas (ALPHA),” Presentation at SAE International Conference on Icing of Aircraft, Engines, and Structures, June 2019.

## Acknowledgments

Many people contributed to the success of these flight campaigns and the authors are grateful to all who helped. Special recognition is due to the entire NASA DC-8 team - particularly Adam Webster, Tim Moes, Ken Norlin, and pilots Nils Larson, Wayne Ringelberg, Dave Fedors, and Frank Batteas for the safe flight operation, to the FAA, particularly Tom Bond, Jim Riley, and Stephanie DiVito for their sustained financial and technical support, to Matt Grzych from Boeing and Ben Bernstein from Leading Edge Atmospheric for their forecast support and real-time tactical guidance. Thanks also are extended NASA Langley satellite team, Louis Nguyen, Chris Yost for adapting to the many changes within this project and to NCAR’s Julie Haggerty for implementation of ALPHA, the data archive, and instrumentation support. The research was sponsored by NASA’s Advance Air Vehicles Program through the Advance Air Transport Technology (AATT) and the Aeroscience Evaluation Test Capabilities (AETC) projects and by the FAA’s Aviation Weather Research Program.

## Definitions/Abbreviations

<b>ADC</b>	Air Data Computer
<b>AFRC</b>	Armstrong Flight Research Center
<b>ALPHA</b>	Algorithm for Predicting High ice water content Areas
<b>ARAC</b>	Aviation Rulemaking Advisory Committee
<b>ATC</b>	Air Traffic Control
<b>BHS</b>	Background Humidity System
<b>CDP-2</b>	Cloud Droplet Probe (DMT)
<b>DLH</b>	Diode Laser Hygrometer
<b>DMT</b>	Droplet Measurement Technologies
<b>EASA</b>	European Aviation Safety Agency
<b>FAA</b>	Federal Aviation Administration
<b>FAR</b>	False Alarm Rate
<b>HAIC</b>	High Altitude Ice Crystal
<b>HIWC</b>	High Ice Water Content
<b>I&amp;Q</b>	In-phase and Quadrature
<b>IAS</b>	Indicated Air Speed
<b>I<sub>D</sub></b>	Index of Dispersion
<b>IR</b>	Infrared
<b>IWC</b>	Ice Water Content
<b>KFLL</b>	Fort Lauderdale/Hollywood International Airport
<b>MCS</b>	Mesoscale Convective System
<b>MEL</b>	Minimum Equipment List
<b>MOPS</b>	Minimum Operational Performance Standards
<b>MSD</b>	Mass Size Distribution
<b>NASA</b>	National Aeronautics and Space Administration
<b>Nm</b>	Nautical Miles
<b>NRC</b>	National Research Council Canada
<b>PIP</b>	Precipitation Imaging Probe (DMT)
<b>POD</b>	Probability of Detection

<b>PPI</b>	Plan Position Indicator
<b>PSD</b>	Particle Size Distribution
<b>RASTA</b>	RAдар SysTem Airborne
<b>R-IWC</b>	Radar Ice Water Content
<b>RRF</b>	Radar Reflectivity Factor
<b>SAFIRE</b>	Service des Avions Français Instrumentés pour la Recherche en Environnement
<b>SAT</b>	Static Air Temperature
<b>SEA</b>	Science Engineering Associates
<b>SLD</b>	Supercooled Large Drop
<b>SPEC</b>	Stratton Park Engineering Company
<b>TAT</b>	Total Air Temperature
<b>TWC</b>	Total Water Content
<b>UTC</b>	Coordinated Universal Time
<b>WVSS-II</b>	Water Vapor Sensing System (SpectraSensor)



## Appendix

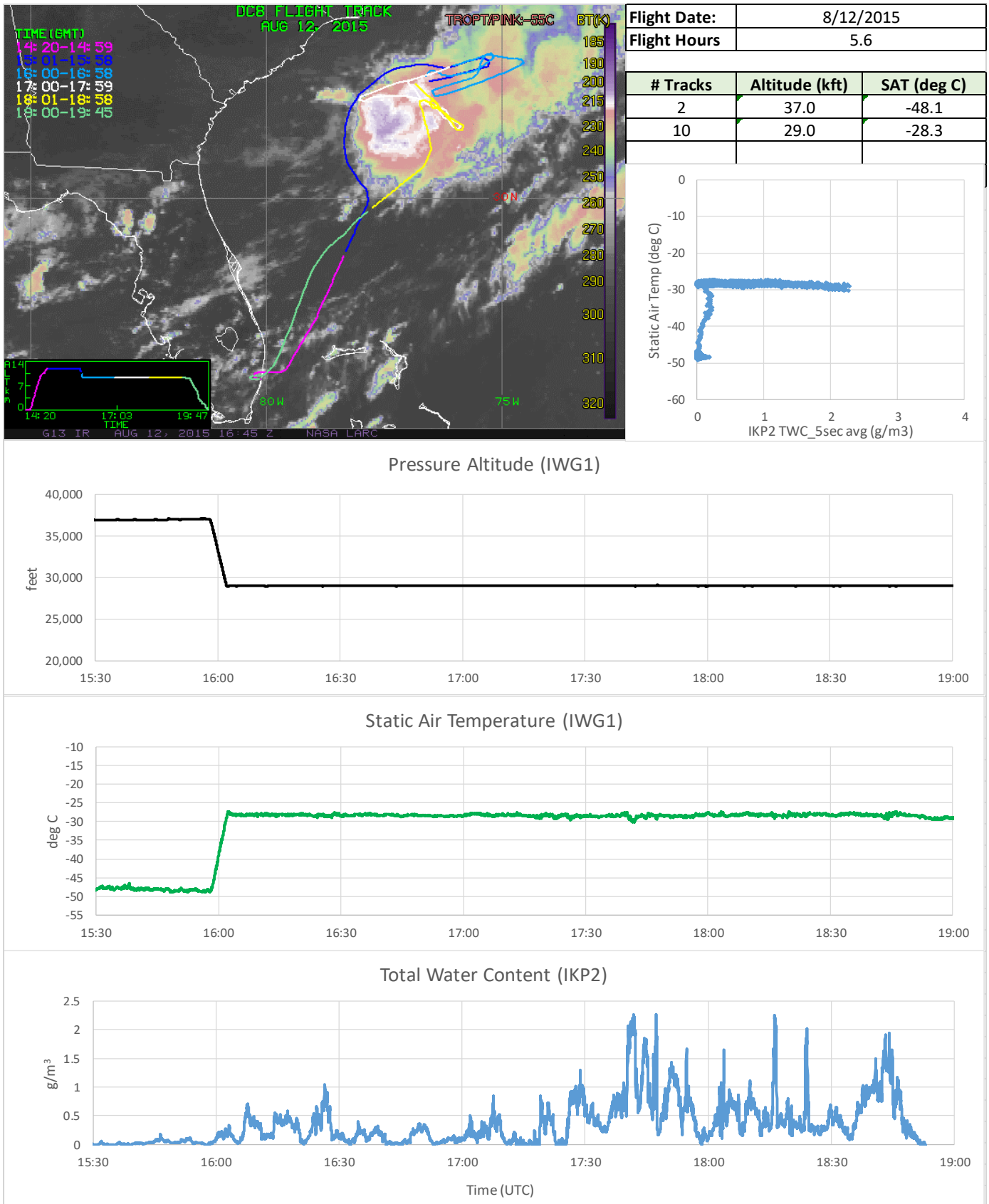


Figure 35. 2015-08-12 Flight track overlay on IR satellite image and select time histories

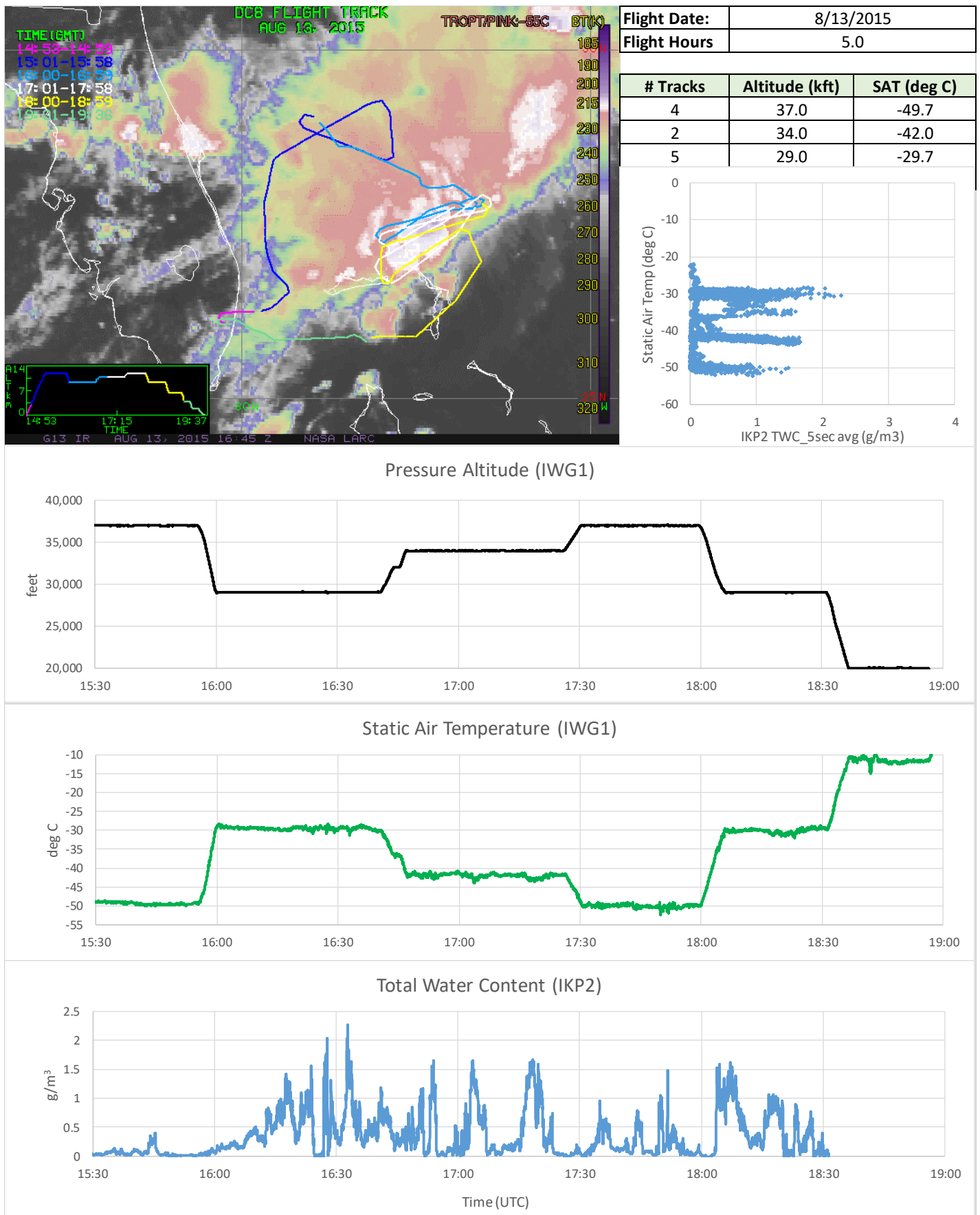


Figure 36. 2015-08-13 Flight track overlay on IR satellite image and select time histories

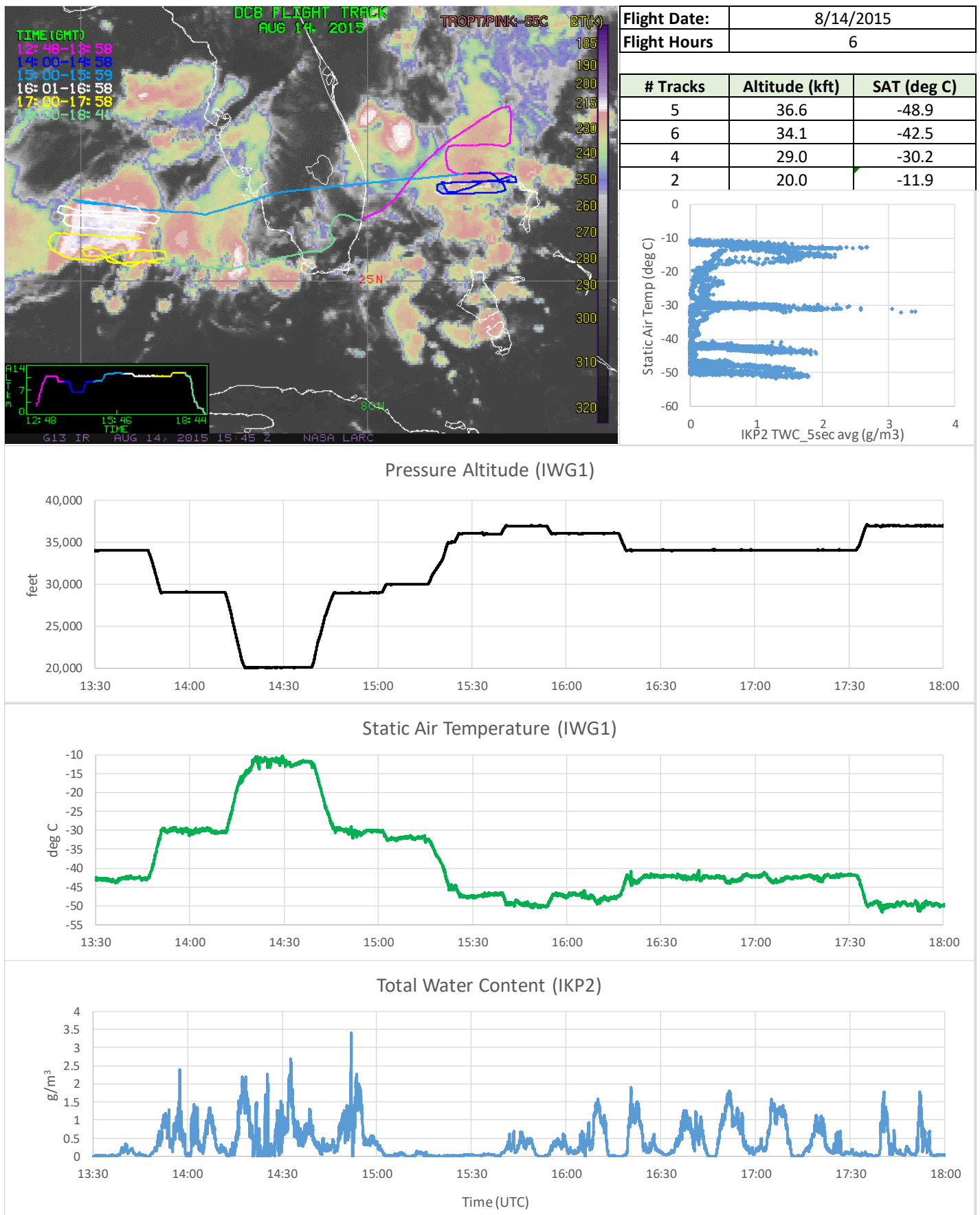


Figure 37. 2015-08-14 Flight track overlay on IR satellite image and select time histories



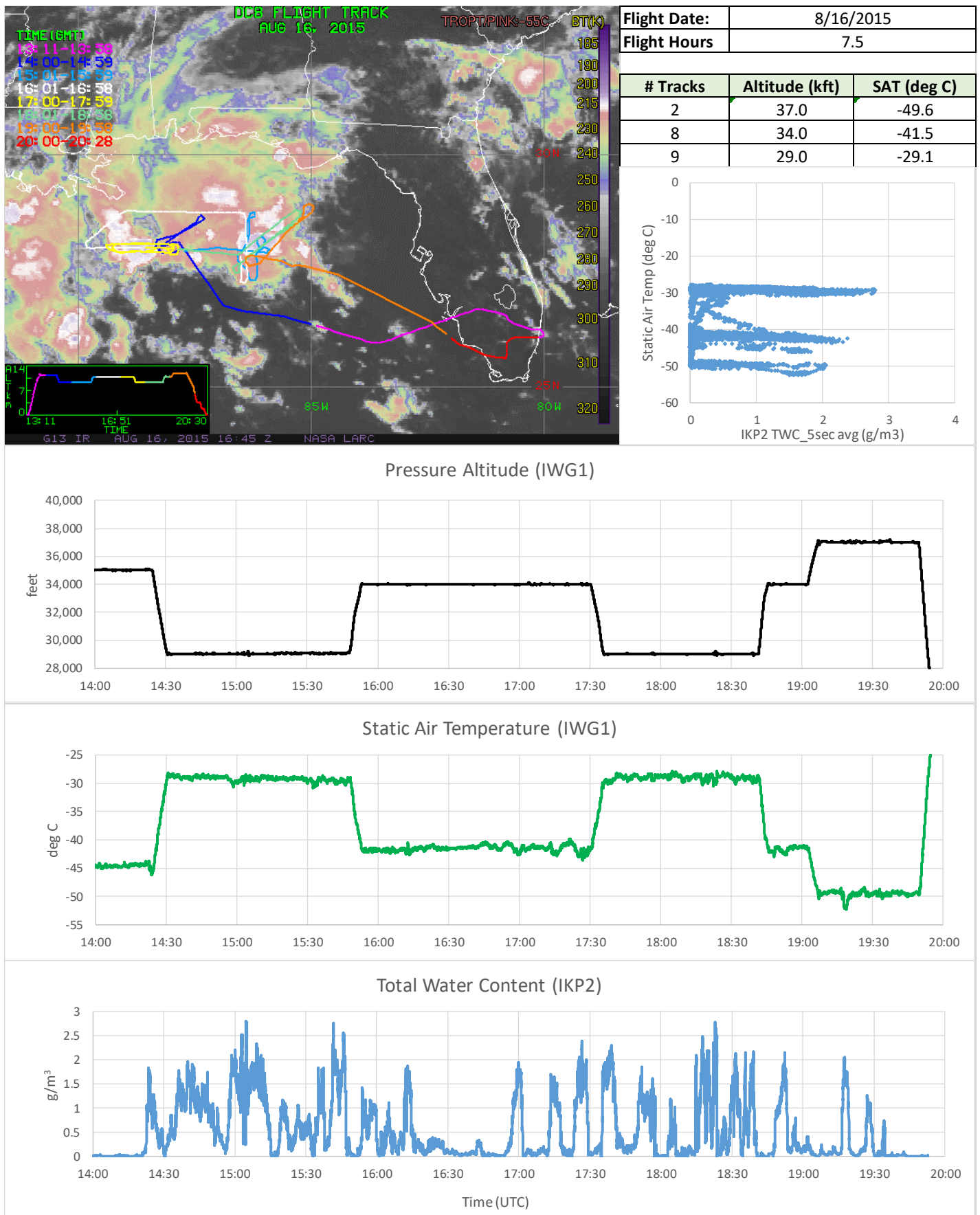


Figure 38. 2015-08-16 Flight track overlay on IR satellite image and select time histories

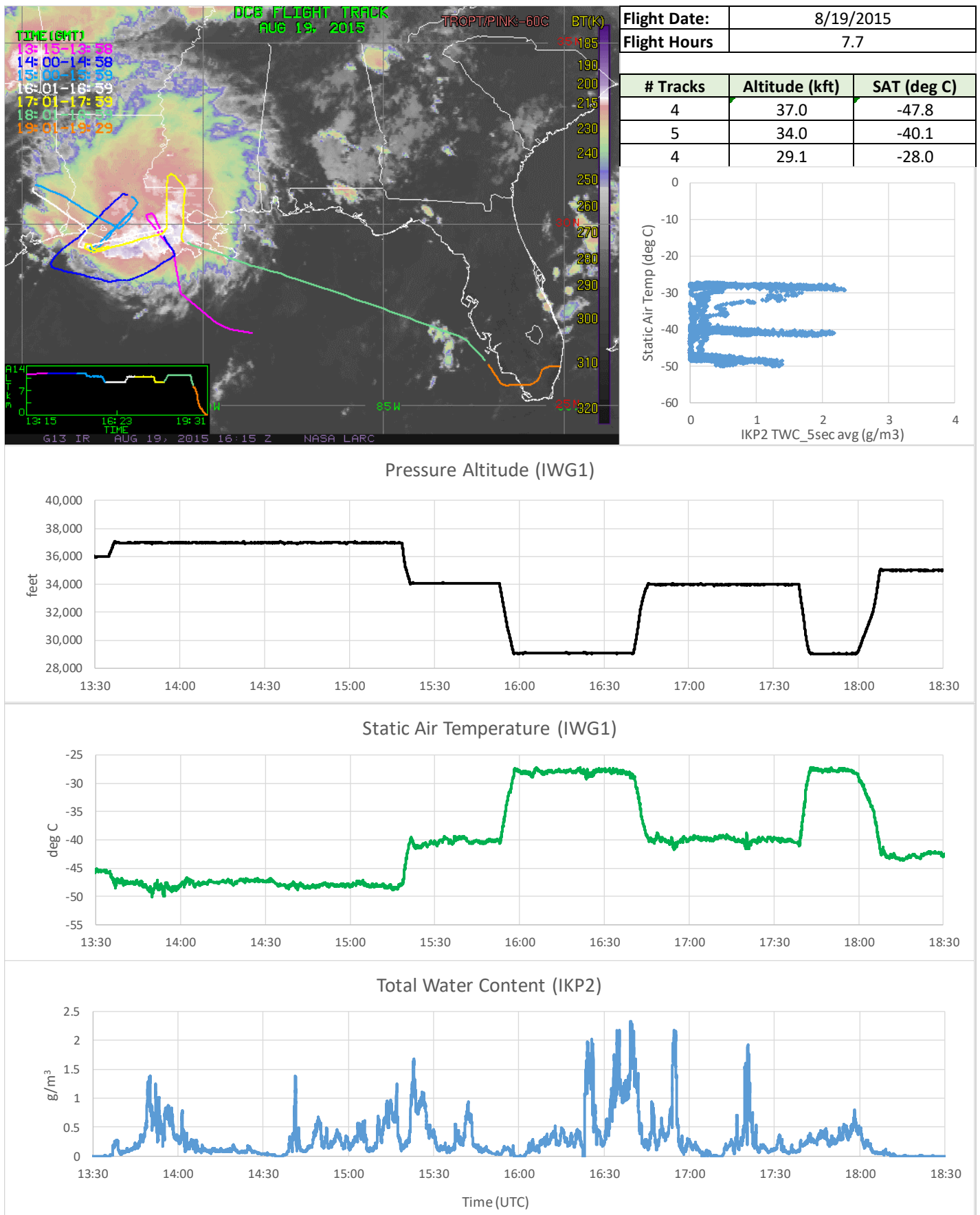


Figure 39. 2015-08-19 Flight track overlay on IR satellite image and select time histories

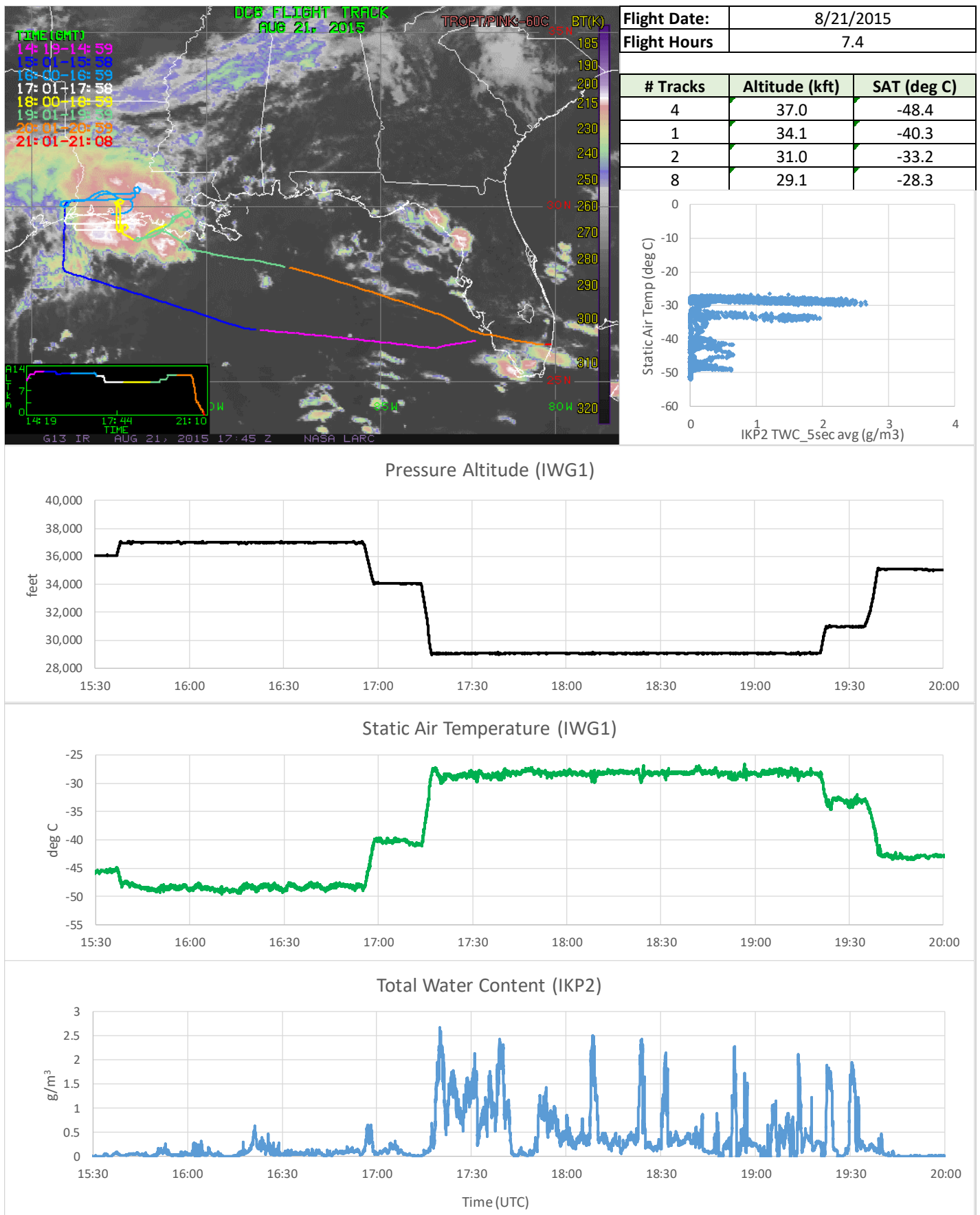
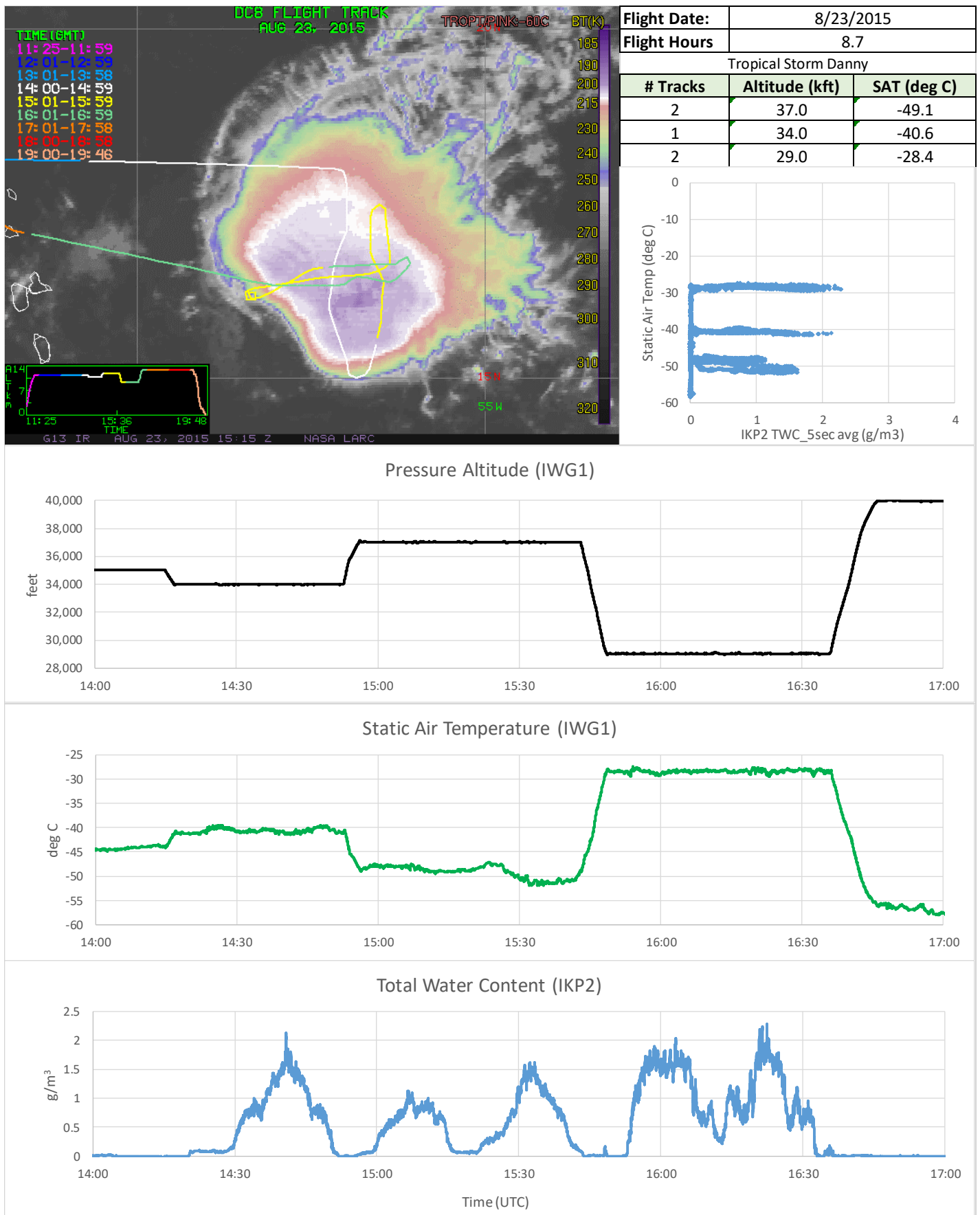


Figure 40. 2015-08-21 Flight track overlay on IR satellite image and select time histories





*Figure 41. 2015-08-23 Flight track overlay on IR satellite image and select time histories*

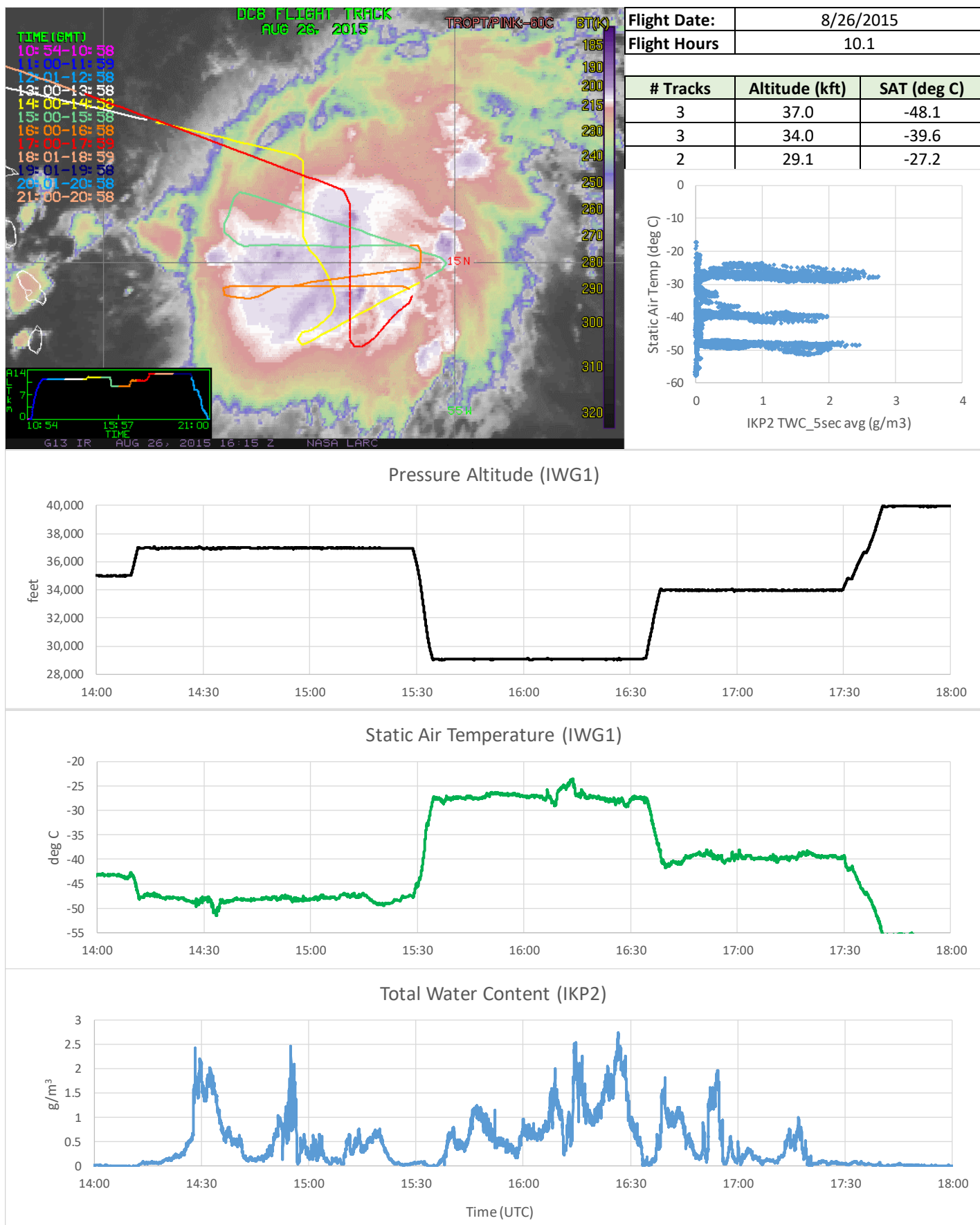


Figure 42. 2015-08-26 Flight track overlay on IR satellite image and select time histories

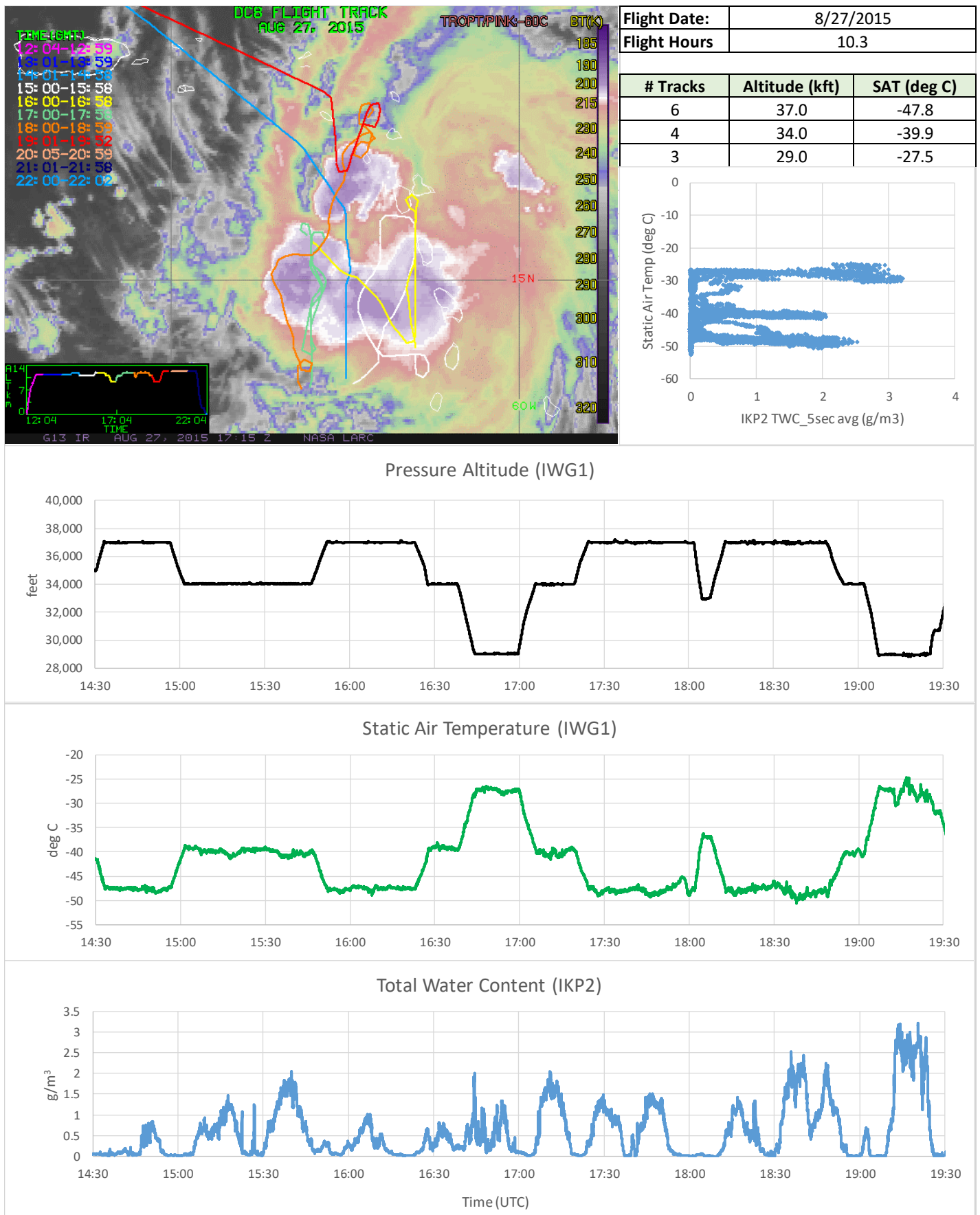


Figure 43. 2015-08-27 Flight track overlay on IR satellite image and select time histories



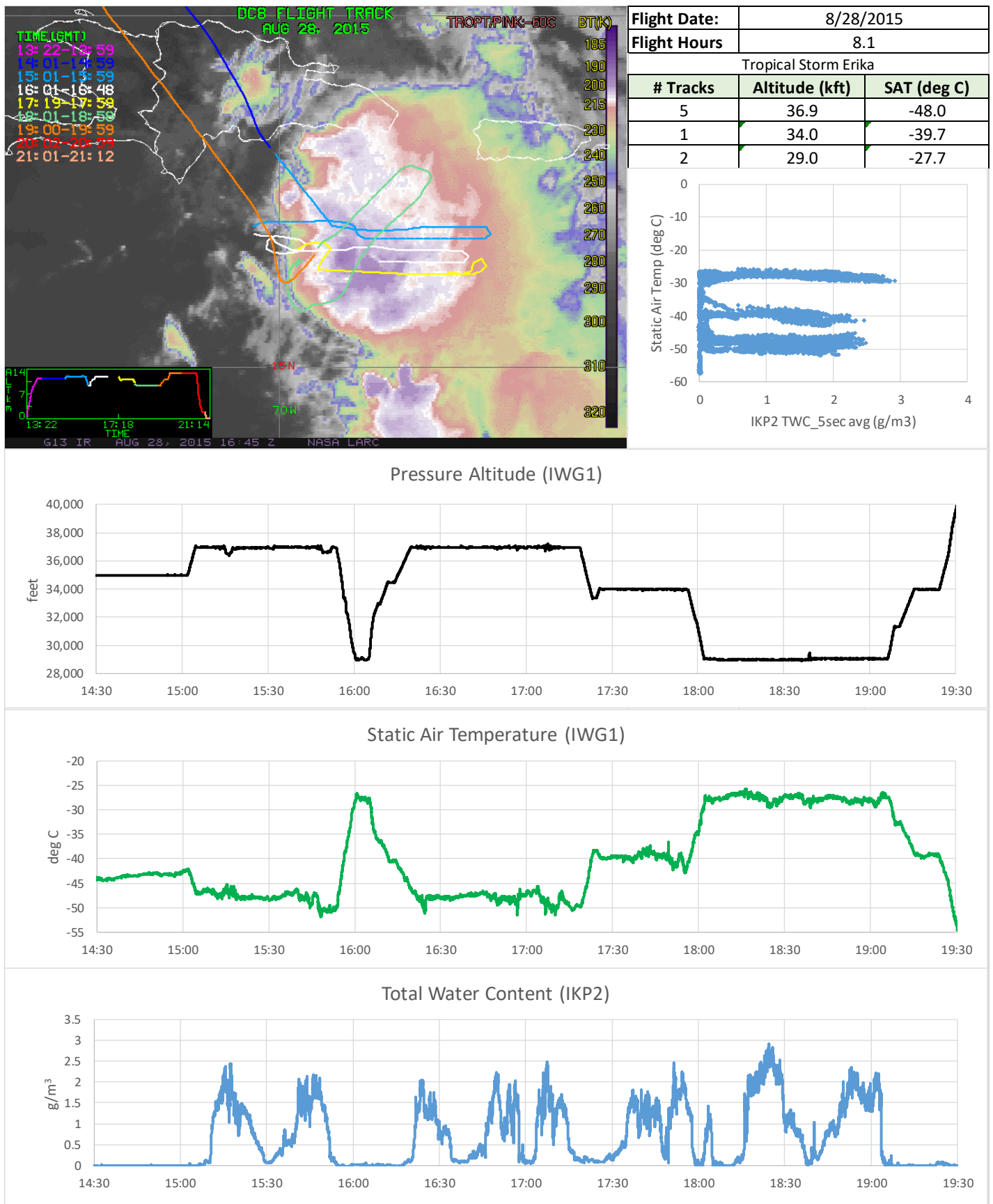
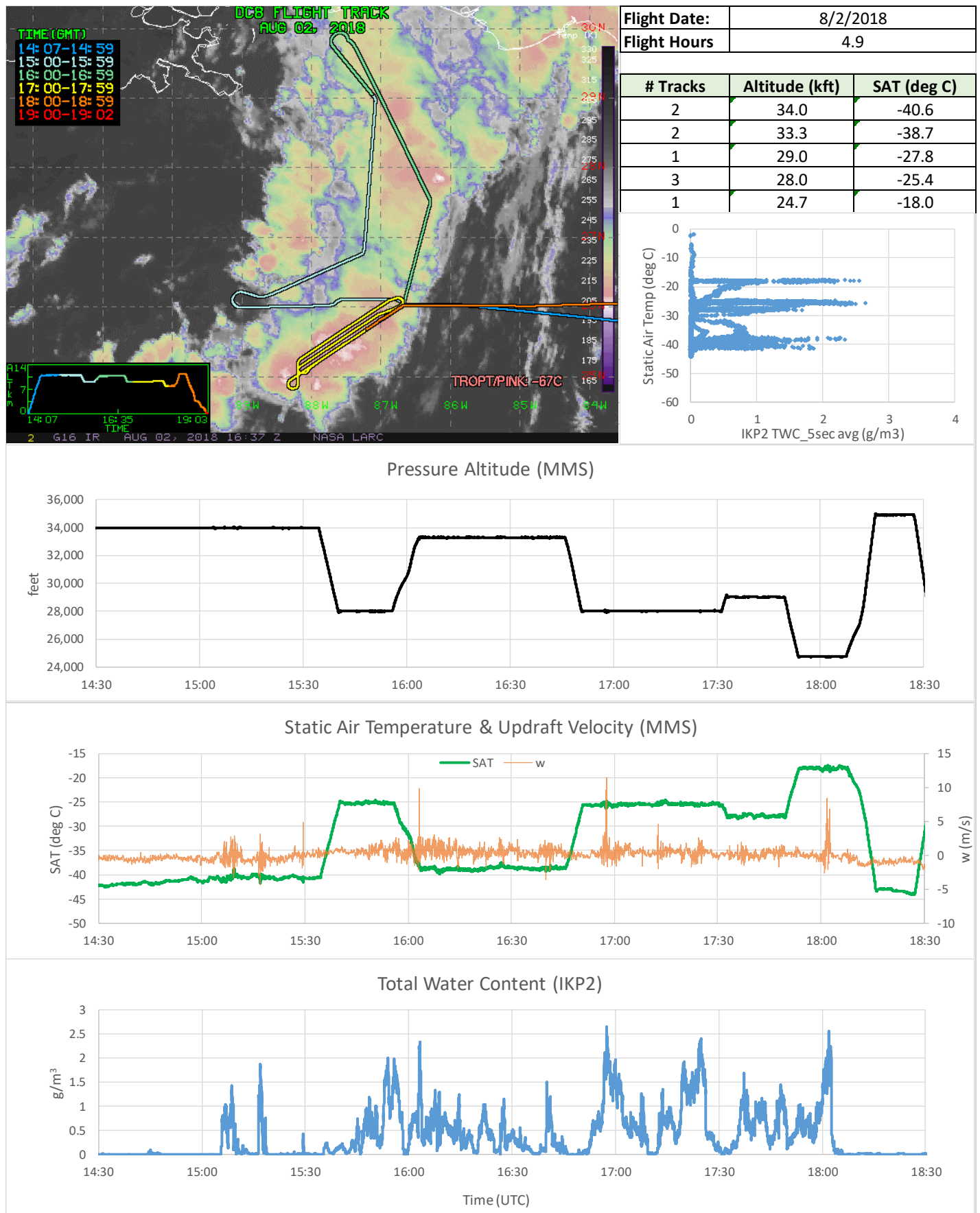
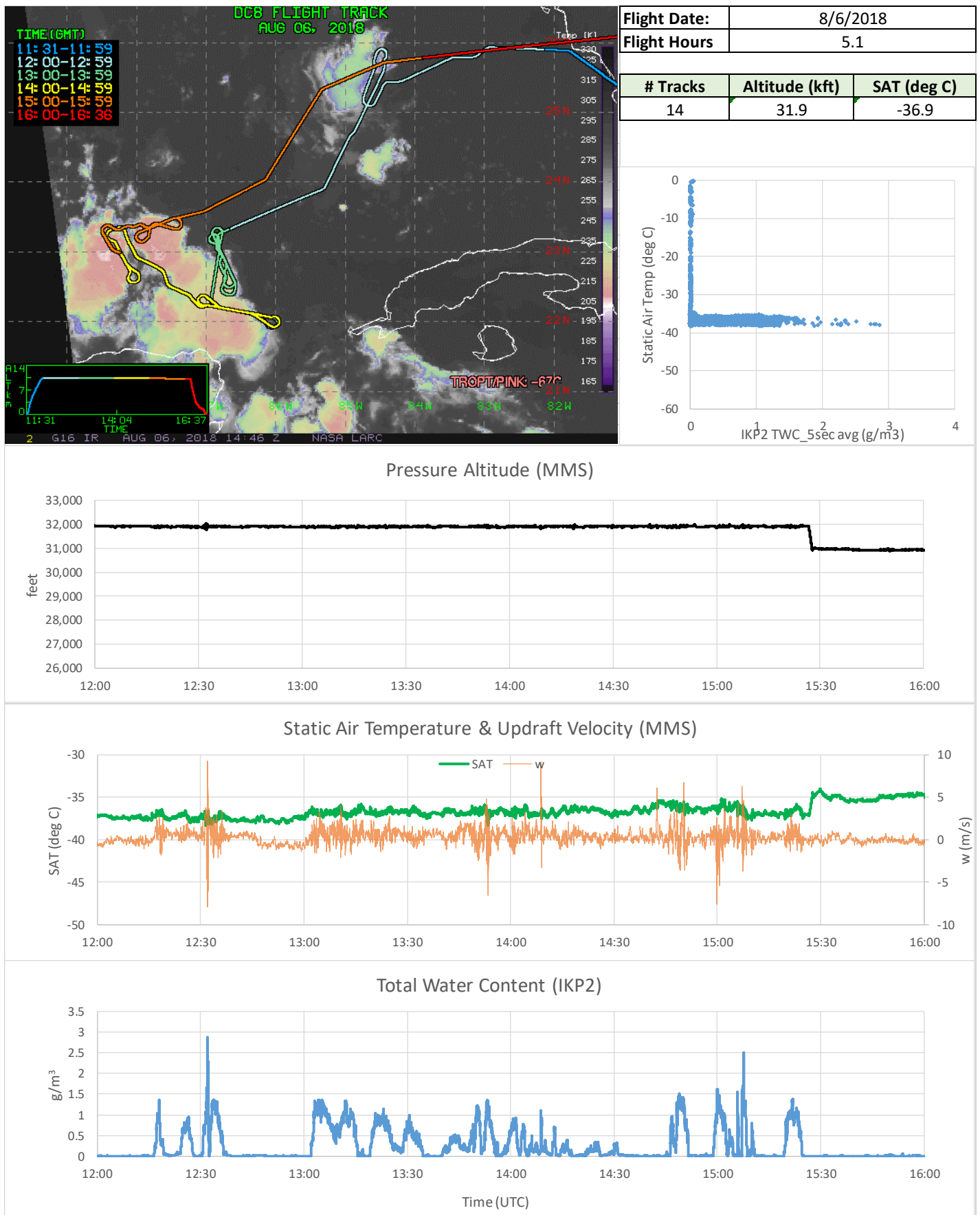


Figure 44. 2015-08-28 Flight track overlay on IR satellite image and select time histories



*Figure 45. 2018-08-02 Flight track overlay on IR satellite image and select time histories*



*Figure 46. 2018-08-06 Flight track overlay on IR satellite image and select time histories*



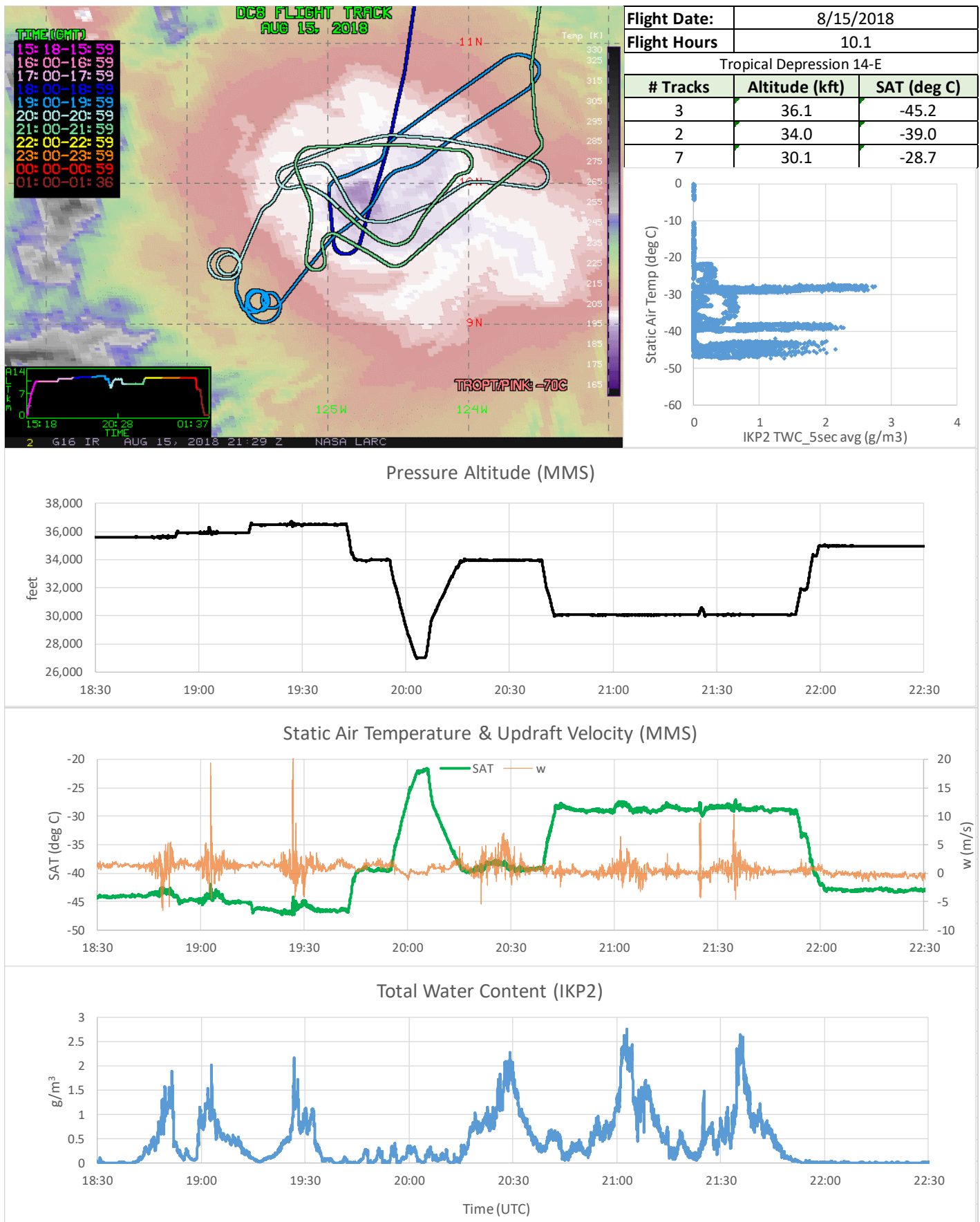


Figure 47. 2018-08-15 Flight track overlay on IR satellite image and select time histories

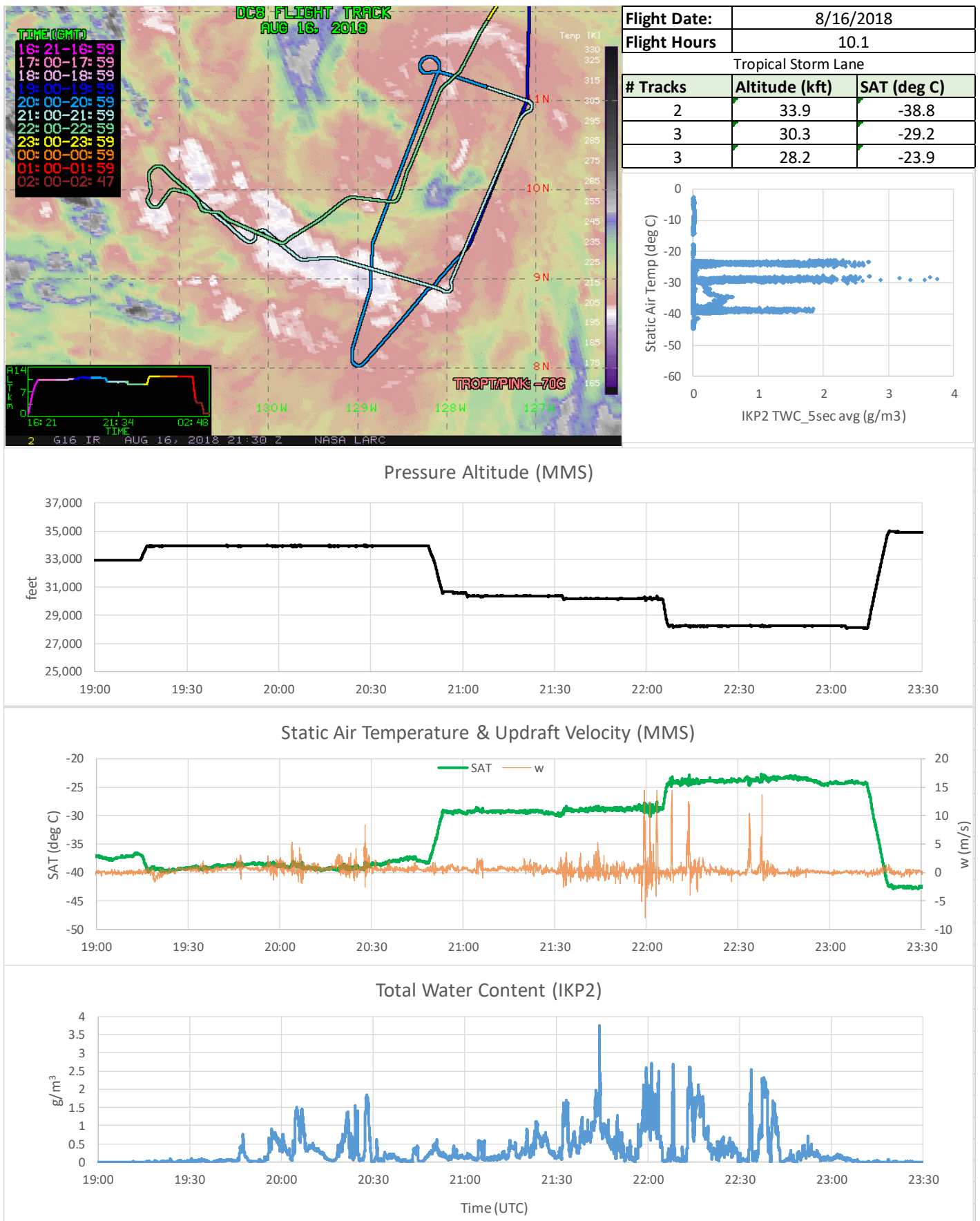


Figure 48, 2018-08-16 Flight track overlay on IR satellite image and select time histories

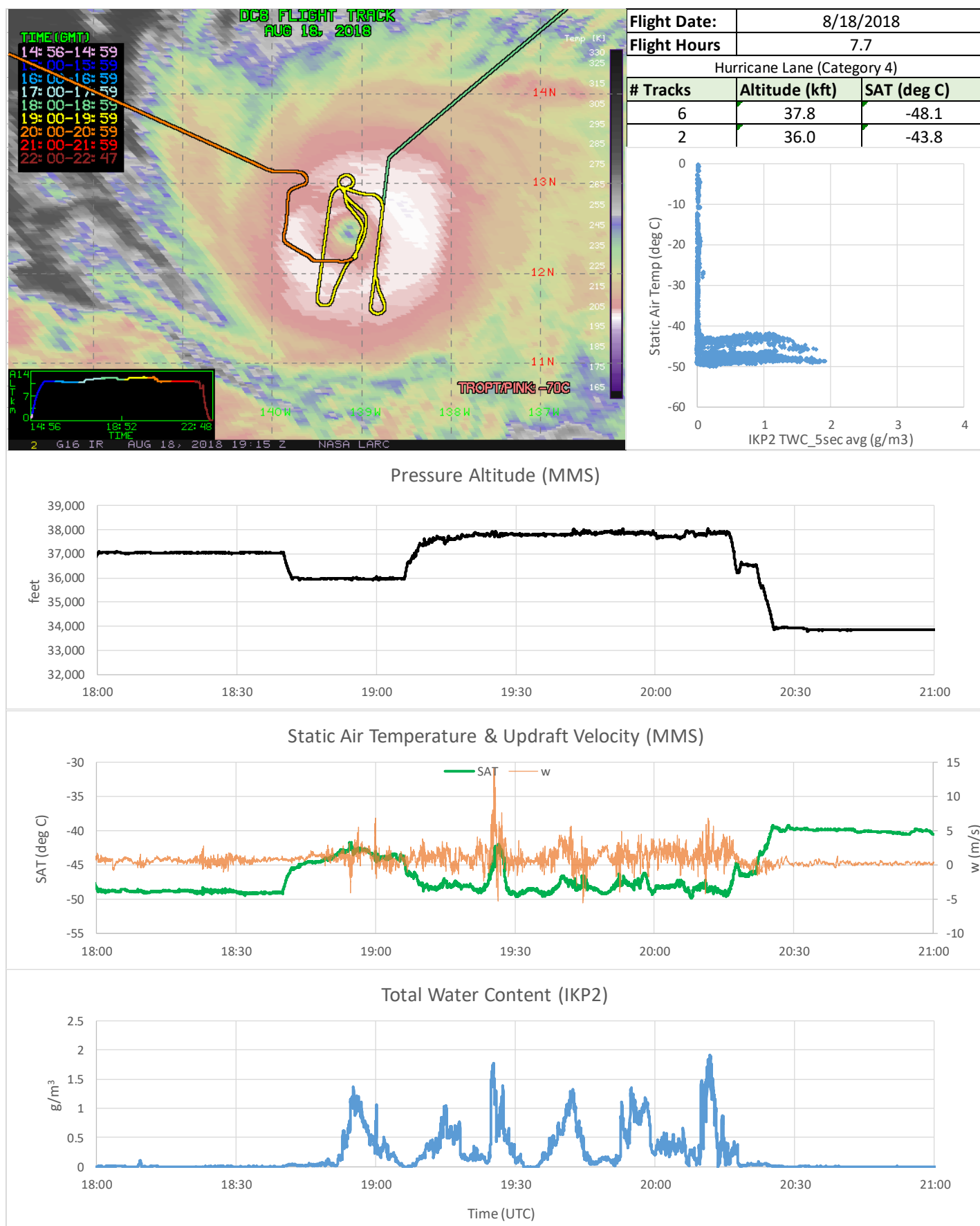


Figure 49. 2018-08-18 Flight track overlay on IR satellite image and select time histories



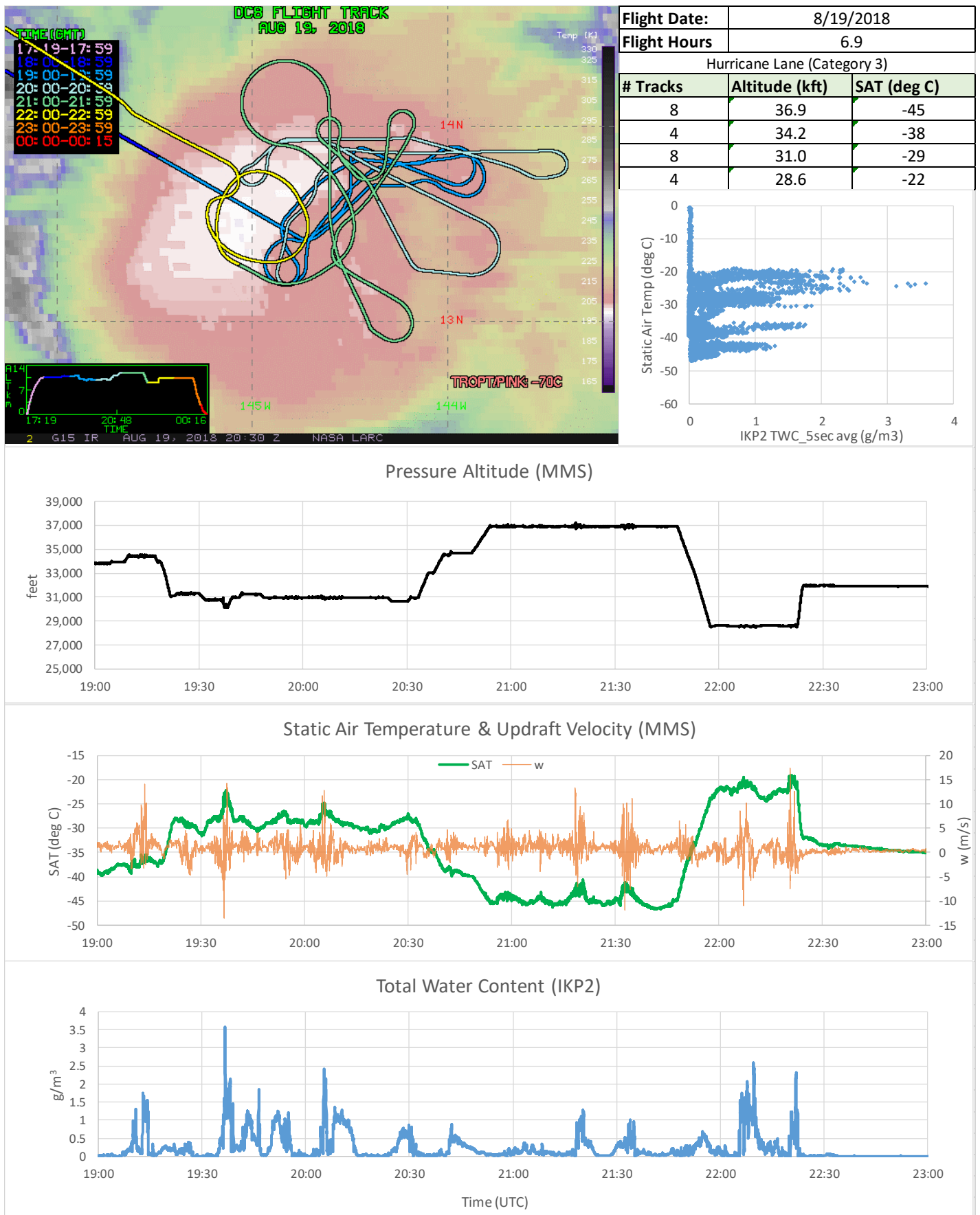


Figure 50. 2018-08-19 Flight track overlay on IR satellite image and select time histories

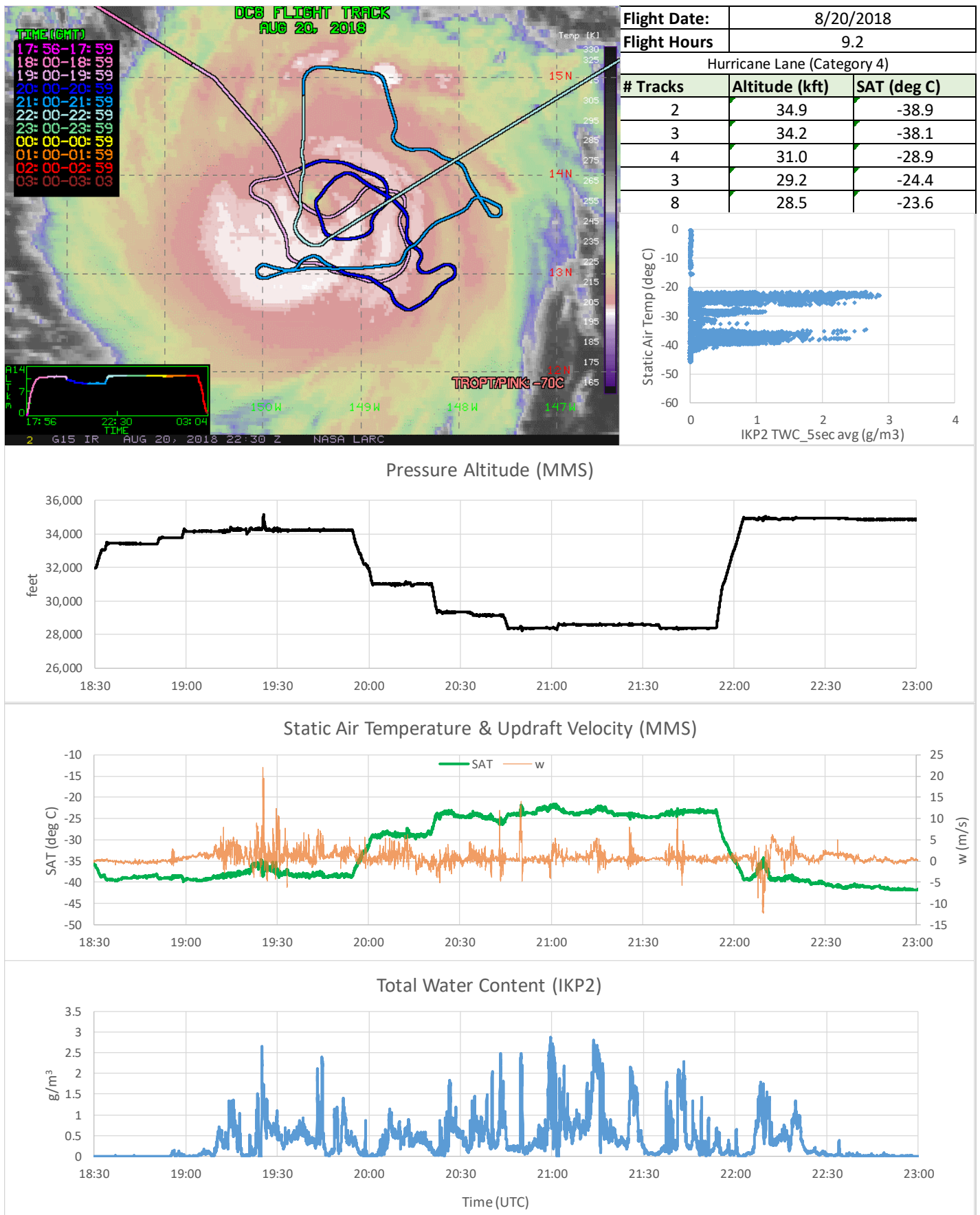


Figure 51. 2018-08-20 Flight track overlay on IR satellite image and select time histories